Special Session, "A tribute to Edilton Santos, a leader in Precambrian Geology in Northeastern Brazil", edited by A.N. Sial and V.P. Ferreira

DOI: 10.1590/2317-4889202020200034

BJGEO Brazilian Journal of Geology

Geology, geochronology Pb-Pb, U-Pb-Hf zircon and Sm-Nd T_{DM} of the Uruburetama batholith, Northern Borborema Province: contextualization in the Santa Quitéria Magmatic Arc

Paulo Sergio de Sousa Gorayeb[1]*, Luana Camile Silva-Silva[1], Marco Antonio Galarza[1,2]

Abstract

Records of large crustal masses in the northwest of Borborema Province (BP) spread over more than 300 km are found as numerous granitic bodies amid a high-grade metamorphic gneissic-migmatitic terrain. The Tamboril-Santa Quitéria Complex (TSQC) is a Neoproterozoic example of these records; it is located in the north of the Ceará Central Domain (CECD) and its origin is related to a continental magmatic arc at different evolutionary stages of the arc. The Uruburetama Granite (UG), object of this study, fits into this context and constitutes one of the most representative batholiths occupying an area of 1,500 km^2. Dozens of other similar plutons have been recorded in cartographic works that show similarities which suggests the grouping of these bodies in the Uruburetama Granitic Suite (UGS), previously included in the TSQC. The UG consists of a variety of plutonic rocks associated with mafic-dioritic dikes and its metamorphic products. Six petrographic facies were identified among the plutonic rocks: biotite-hornblende monzogranites and syenogranitic varieties, biotite-hornblende granodiorites, in addition to quartz syenite, leucomonzogranites, and diorites rocks. These rocks are affected by deformation, with greater intensity at the edges of the batholith, where thrust shear zones with transcurrent components were installed, generating tectonic fabrics (mylonitic foliations, stretch lineation, almond feldspar porphyroclasts, and ribbon quartz). Despite the superimposed deformational effects, magmatic relict textures are partially preserved, mainly toward the central portion of the pluton. The UG and the associated plutons are hosted by migmatized orthogneisses, paragneisses with garnet, sillimanite or kyanite, marbles, calcium-silicate gneisses, micaschists, sillimanite quartzites, and amphibolite lenses. The contact relations are diffuse with gradation for migmatites, and in rare cases, intrusive contacts with gneiss mega-xenolites are registered. The geochronological data obtained by Pb-evaporation zircon in two samples of the UG show average ages of 655 ± 2 and 656 ± 1 Ma. U-Pb zircon data for the same samples showed slightly younger age values of 559 ± 10 and 634 ± 10 Ma, respectively. The ages obtained are considered as representative of the magmatic phases of UG crystallization in the context of the evolution of the Santa Quitéria Magmatic Arc (SQMA), with the main magmatic phase of the UG in the Cryogenian. However, the age of 559 Ma would represent a younger magmatic event in the evolution of the arch. Overall, these ages correspond to the "Pre-Collisional I" or "Early-Sin-Orogenic" phase of a large collisional belt in the west of BP, and the younger ages must represent events related to the continuity of the orogen convergence of the Latest-Pre-collisional I (634 Ma) and Post-Collisional I (559 Ma) phases. Sm-Nd whole-rock isotopes data showed $\varepsilon_{Nd}(t)$ values predominantly negative (-25.6 and -0.9), and Nd-T_{DM} model ages of 2.90 and 1.2 Ga. The results of the Lu–Hf isotopes analysis for the Bt-Hbl monzogranite sample showed negative ε_{Hf} values (-26.75 to -35.48) and Hf-T_{DM}^{C} model ages of 3.12 to 3.65 Ga while the results for Bt-Hbl granodiorite showed ε_{Hf} values of -2.07 to +1.08 and Hf-T_{DM}^{C} model ages of 1.46 to 1.66 Ga. These data point to the existence of two distinct and older crustal sources in the generation of these granitoids, one in the Mesoarchean, and the other in the Mesoproterozoic. The Archean ages correspond to the basement in the south of the CECD (Tróia Massif and Granjeiro Complex); on the other hand, the Mesoproterozoic ages are up for discussion, since terrains with this type of age do not occur adjacent to the BP. On the other hand, it can be interpreted as a mixture of sources, one of them probably juvenile, neoproterozoic, with contamination of the Archean crust. Thus, the UG is considered one of the most important records of the beginning of the evolution of the Santa Quitéria Magmatic Arc associated with a wide collisional belt in the "West Gondwana Orogen" in the west of Borborema Province.

KEYWORDS: Pb-Pb and U-Pb-Hf geochronology in zircon; Sm-Nd T_{DM}; Uruburetama Batholith; Santa Quitéria Magmatic Arc, NW-Borborema Province; West Gondwana Orogen.

INTRODUCTION

Records of large crustal masses in the form of granitic plutons of varying dimensions, compositional types and ages reveal, in the northwest of Borborema Province (BP), a strip of Neoproterozoic granitoids spread over more than 300 km, amidst high metamorphic gneissic terrain in northwestern Ceará State, whose main plutons are Uruburetama, Manoel Dias, Mirindiba, Extrema, Aracatiaçu, Tamboril, and Nova Russas granites (Figs. 1A and 1B).

Most of these granitic bodies can be observed in the Geological Map of Ceará State (Cavalcante *et al.* 2003) and in other more recent cartographic surveys (Gorayeb *et al.* 2014, Naleto 2018, Braga 2017).

In the literature and geological maps of the Geological Survey of Brazil (*Companhia de Pesquisa de Recursos Minerais* — CPRM) (Cavalcante *et al.* 2003, Naleto 2018, Gorayeb *et al.* 2014), there is no formal name for these granitic bodies being generically referred to as "Granitoids of the Tamboril-Santa

[1]Universidade Federal do Pará – Belém (PA), Brazil.
E-mails: gorayebp@ufpa.br; luana.silva@ig.ufpa.br; antogt@ufpa.br
[2]Laboratório Pará-Iso, Universidade Federal do Pará – Belém (PA), Brazil.
*Corresponding author.

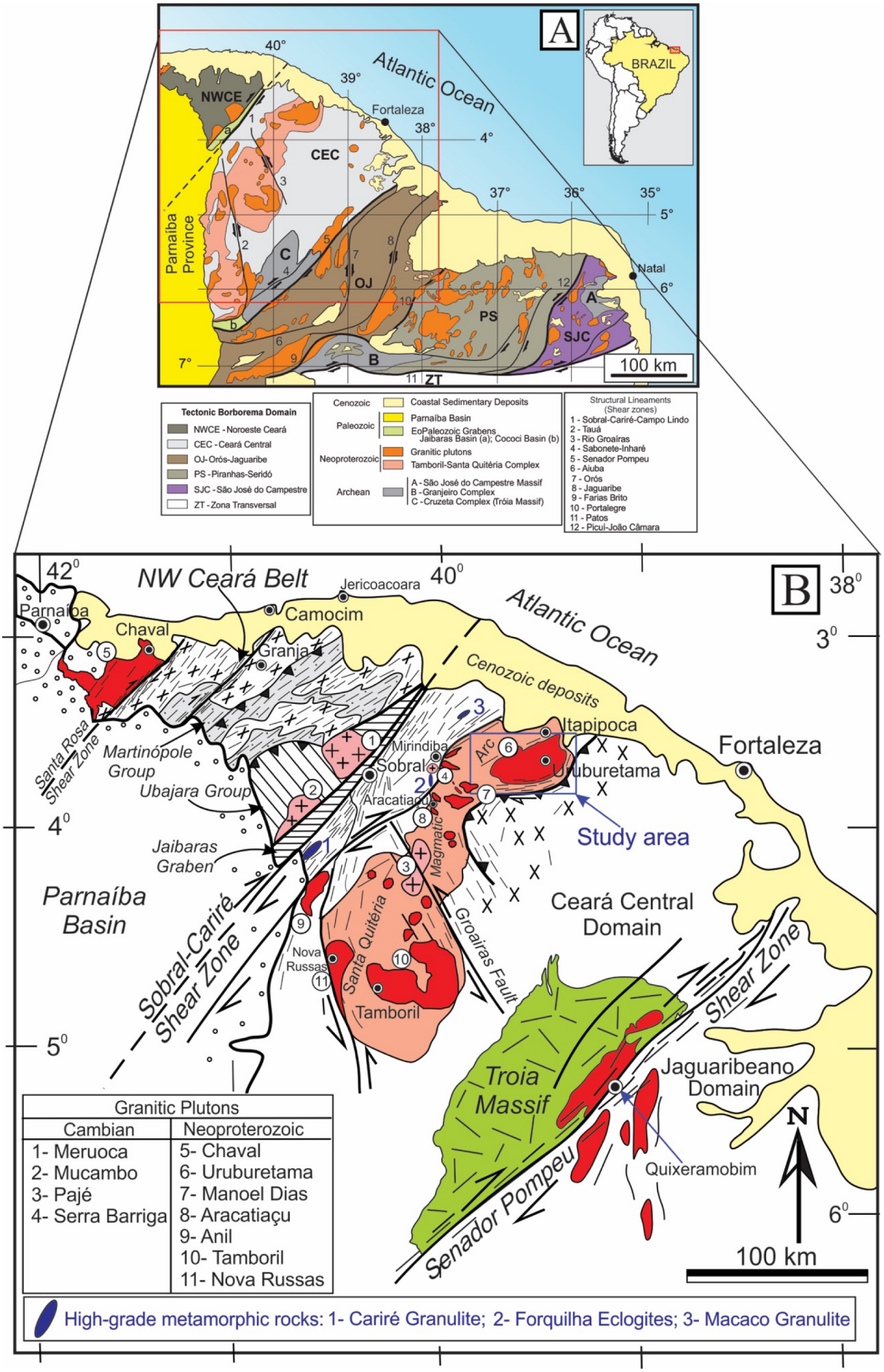

Figure 1. (A) Geological map of northern Borborema Province with the geotectonics domains, adapted from Naleto (2018); (B) geological map of the northwest of Borborema Province with the main geologic-geotectonics units, indicating the study area (modified from Cavalcante *et al.* 2003).

Quitéria Complex", "Santa Quitéria Unit", and "Tamboril Unit". Therefore, in this work, they are proposed to be brought together in the Uruburetama Granitic Suite (UGS).

Regional geochronological studies have led to the definition of a continental magmatic arc, named Santa Quitéria Magmatic Arc (SQMA), related to the evolution of the Brasiliano Cycle widely registered in the Borborema Province (Fetter *et al*. 2003, Santos et al. 2008, Ganade Araujo *et al*. 2014a, 2014b).

On the other hand, despite extensive geological knowledge, there are no specific nor more detailed studies on the various plutons; there is also no petrological, geochronological, and isotopic data that characterizes them, as they are geologically complex with records of successive magmatic and tectono-metamorphic processes in their evolution.

Thus, with the advancement of cartographic knowledge in the region and the diversity of Neoproterozoic granitogenesis events, a more detailed study of these plutons is necessary, to individualize the bodies, define their petrographic, geochemical, and typological nature along with a systematic geochronological and isotopic study to identify the magmatic events and their origins.

The northern portion of the SQMA has one of the most expressive and representative granitic bodies in the region, the Uruburetama Batholith, with great exposure in the Uruburetama mountain range, accompanied by several other smaller bodies, in the north of the CECD (Fig. 1). The present study focuses on this body, for the reasons reported above, and also, due to the few aggregated knowledge, large exposure area, difficult access and its importance as part of this arc magmatism in the context of the BP granitogenesis.

The study area is located in the north of Ceará State, Northeast Brazil, having as reference the cities of Uruburetama, Itapipoca, Itapajé, Irauçuba, and Umirim, located in Irauçuba (SA.24-YDV) and São Luiz do Curu (SA.24-YD-VI) charts, and is delimited by the coordinates 3°47'–3°52' S and 39°55'–39°20' WGr (Fig. 1).

In the present work, field surveys were carried out on the pluton of great cartographic expression (Uruburetama Granite — UG) and other adjacent bodies that can be observed in the Irauçuba and Sobral charts (Naleto 2018, Gorayeb *et al*. 2014), and involved the collection of structural data, definition of spatial-temporal relations with country rocks, and systematic collection of representative samples of their petrographic varieties. These additional data enabled the petrographic characterization of the granitoids, textural/microstructural analysis; correlations with other bodies and interpretation of the emplacement of those bodies tectonically.

In addition, the work presents new geochronological and isotopic data using the Pb-evaporation/ionization methods in zircon, U-Pb and Lu-Hf in zircon and Sm-Nd T_{DM}, which allowed the definition of the age of crystallization of the body, interpretation about the granitoids sources and discussion of correlations with granitogenesis events defined in the BP. Data from other plutons were collected in the CPRM mapping work, in cartographic work carried out by the Faculty of Geology of the Universidade Federal do Pará (UFPA) and in various publications in the region.

ACTIVITIES AND METHODS

For the development of this study, a bibliographic survey was initially carried out on the geology of the northwestern portion of the BP, more specifically the Ceará Central Domain (CECD) with an emphasis on neoproterozoic granitogenesis. A geological and logistical cartographic base of the region was elaborated, structured in a Geographic Information System (GIS), based on the interpretation of satellite images and other remote sensor products.

For the elaboration of the geological map, cartographic data from SA.24-YDV (Irauçuba) chart were used in the scale of 1:100.000 (Naleto 2018), and data from the geological mapping of the Umirim Project, carried out in 2012 by the Faculty of Geology (*Faculdade de Geologia* — FAGEO) of the Geosciences Institute (*Instituto de Geociências* — IG) of UFPA on a scale of 1:25,000.

The geological map was made from shape-files of the referred project, adding the data collected in the fieldwork of the present study, using the ArcGIS® 10.1 software. These works were developed at the Laboratory of Image Analysis of the Humid Tropics (*Laboratório de Análise de Imagens do Trópico Úmido* — LAIT) of IG/UFPA.

Then, field surveys were carried out to collect geological data, with observation and systematic data collection and structural measures in 23 key outcrops, and sample collection for petrographic, geochronological, and isotopic studies. In addition, 25 samples from the IG/UFPA collection were also described.

Petrographic analyzes were carried out at the FAGEO Petrography Laboratory, using 30 hand samples and corresponding thin sections. For the modal analysis, the Swift Point Counter of the Petrography Laboratory (*Laboratório de Petrografia* — LAPETRO) of the Graduate Program in Geology and Geochemistry (*Programa de Pós-Graduação em Geologia e Geoquímica* — PPGG) was used, following the procedures of Chayes (1956) and Hibbard (1995). 1,200 points were counted with 2 spacings, for each sample, using the data for classification of granites in the quartz-alkalifeldspar-plagioclase (QAP) diagram following the recommendations of Streckeisen (1976) and Le Maitre (2002), as established by the International Union of Geological Society (IUGS).

The geochronological studies were performed initially by the radiometric dating method Pb-evaporation-ionization and later U-Pb in zircon crystals. Isotopic studies were complemented by model-ages Nd-T_{DM} (whole-rock) and Hf-T_{DM}^{C} (zircon).

Analytical details of the geochronological and isotopic methods will be presented in the specific section.

REGIONAL GEOLOGICAL CONTEXT

The CECD, where the study area is located, is part of the northern portion of the BP (Almeida *et al*. 1981) presenting, in the southern portion, the Tróia Massif, which represents an old Archean inlier of 2.86–2.79 Ga (Fetter 1999), bringing together tonalite-trondhjemite-granite (TTG) suites and greenstone association which is involved by Paleoproterozoic orthogneisses of the Cruzeta Complex and magmatic-sedimentary sequences with representatives of the Algodões and

Madalena units (2.17–2.13 Ga) (Fig. 1) (Fetter *et al.* 2000, Arthaud *et al.* 2007, Martins *et al.* 2009, Costa *et al.* 2018).

All these crustal segments constitute the ancient basement, on which Neoproterozoic supracrustal volcano-sedimentary units represented by the Ceará Complex and the Novo Oriente Group (Arthaud *et al.* 2007, Ganade Araujo *et al.* 2012b) were established.

According to Caby and Arthaud (1986), the entire supracrustal ensemble, including the basement, was deformed and metamorphosed at the Brasiliano event (Neoproterozoic) which marked the amalgamation of the Western Gondwana supercontinent. This event occurred under high-grade metamorphic conditions, with wide domain of the sillimanite zone with generalized migmatization, reaching locally high-pressure granulite facies with relict of eclogite facies (650–640 Ma) (Gorayeb and Abreu 1989, Castro 2004, Santos *et al.* 2009, Amaral 2010, Amaral *et al.* 2012), representing the roots of a Neoproterozoic orogen.

The global structural framework reveals a tectonic system of nappes with foliations and stretch lineations from low plunging angles, in a main tangential, collisional tectonic phase. In the most evolved deformational increments, the crustal masses transferred in large dextal NNE-SSW transcurrent shear zones. The main corridors for accommodation of the deformation are the Sobral-Cariré-Campo Lindo and Senador Pompeu shear zones, which delimit the CECD, in addition to several other less significant zones, whose effects reached the whole set at the end of the Neoproterozoic (Arthaud and Torquato 1989, Gorayeb and Abreu 1989, Arthaud 2007, Ganade Araujo *et al.* 2014b).

Another important unit in the northwest of the CECD is the Neoproterozoic Tamboril-Santa Quitéria Complex (TSQC), which is spread over a wide strip for almost 500 km in length and 70 km in width, oriented approximately N-S, from the city of Tamboril to the south and to Uruburetama and Itapipoca to the north. From the Aracatiaçu city, it forms a great arc heading toward ENE, where it is flanked by supracrustal rocks of the Ceará Complex (Fig. 1) (Cavalcante *et al.* 2003).

The TSQC brings together an association of anatectic granitoids in multiple intrusions, mixed with tonalitic, granodioritic and quartz-dioritic orthogneisses, and migmatized paragneisses (metatexites), with the set surrounded by high-grade metasedimentary rocks of the Ceará Complex. The plutons display syn- to late-cinematic deformation that was in part coeval with the injection of younger and less deformed magma (Arthaud *et al.* 2008). In general, they have a wide compositional range from diorites, tonalites, granodiorites to granites, with a predominance of monzogranitic types (Ganade Araujo *et al.* 2012b). Granitoid dating points to an age range of 640 to 610 Ma (Castro 2004, Costa *et al.* 2013, Fetter *et al.* 2003, Ganade Araujo *et al.* 2012b, Santos *et al.* 2008).

Nd isotopic signatures indicate variable mixtures between juvenile Neoproterozoic magmas and older basement, leading to hybrid fonts (Fetter *et al.* 2003). The tectonic context of these granitoids has been interpreted as a Neoproterozoic Andean-type magmatic arc (Fetter *et al.* 2003), but other studies discuss a collisional tectonic evolution of Himalayan-type pointing to an arc at ca. 850 to 640 Ma (Ganade Araujo *et al.* 2012a, Costa *et al.* 2013).

The geochronological and isotopic data presented by Ganade Araujo *et al.* (2014a) allowed the distinction of three different lithological/temporal groups representing magmatic plutons:

- Tonalitic/granodioritic orthogneisses at ca. 880–830 Ma;
- More mafic tonalitic orthogneisses at ca. 650 Ma;
- Orthogneisses at ca. 630 Ma.

The regional structural framework registers foliations with NNE-SSW directions with great inflection in the northeast portion, modifying it to E-W, and low to moderate dips (40°), for opposite quadrants, but wide folds modify this pattern. However, along the contact of the plutons with the gneisses, the stretching lineation plunges gently ENE and has a low rake indicating a dextral strike-slip movement.

Ganade Araujo *et al.* (2014a) reported a large batholith in the central portion of the TSQC, under the informal denomination of "Santa Quitéria Unit", that mainly comprises porphyritic K-feldspar monzogranites which are involved by migmatized orthogneisses, establishing a gradational transition with the gneisses and migmatites (diatexites) of "Tamboril Unit". They also report the existence of local disrupted coeval mafic/intermediate syn-plutonic dykes.

In the work of Bizzi *et al.* (2003), Fetter *et al.* (2003), and Ganade Araújo *et al.* (2012a), the granitogenesis events of the BP were individualized in a succession of magmatic pulses in chronological order in relation to the Brasiliano tectonic event.

Bizzi *et al.* (2003) grouped Neoproterozoic granitic magmatism into a hierarchy of supersuites described below:

- Supersuite I (Early syn-orogenic): represents granites affected by compressive deformation, often exhibiting gneissic or migmatitic structure, such as the TSQC. Fetter *et al.* (2003) obtained U-Pb ages in zircon in migmatized tonalites and granodiorites of this suite of 622 Ma and Sm-Nd model ages (T_{DM}) varying between 0.9 and 1.16 Ga, attributing the emplacement of the bodies to a magmatic arc setting during the compressive regime;
- Supersuite II (Syn to tardi-orogenic): syn-collisional granites are subdivided into tangential syn-tectonics (crustal thickening); and syn-transcurrent (lateral extrusion after thickening). In the CECD, there are two examples of S-type granites, which are the muscovite granites of Senador Pompeu, and the granites of Banabuiú, in the Orós Shear Zone. In the case of granites controlled by mega-transcurrent shear zones, there is the case of the Quixadá-Quixeramobim batholith, with U-Pb in zircon (ID-TIMS) ages at ca 587 ± 5 Ma (Nogueira 2004). Chaval Granite had also been included in this category (U-Pb age in monazite of 591 Ma, Fetter *et al.* 2003), but Aragão *et al.* (2020) obtained new U-Pb zircon data dating in 633 ± 11 Ma, correlating it to the SQMA;
- Supersuite III (Post-orogenic): these granites correspond to the magmatism associated with the dismantling of the Brasiliano orogen, and are well represented by the plutons Tauá, Taperuaba, Morrinhos, São Paulo, and the Meruoca Granitic Suite: plutons Meruoca — 523 ± 5 Ma, Archanjo *et al.* (2009); Mucambo — 532 ± 7 Ma, Fetter *et al.* (2003);

Serra da Barriga — 522 ± 7 Ma, Mattos *et al.* (2007); Pajé — 529 ± 3 Ma, Gorayeb *et al.* (2013); and Aroeiras Dikes — 523 ± 20 Ma, Teixeira *et al.* (2010).

According to Fetter *et al.* (2003) there are four main types of granites related to the development of the magmatic arc, namely:

- Pre-collisional or Type-I: represented by foliated meta-diorites and meta-granodiorites enriched in MgO, with porphyritic texture (megacrystals), metamorphosed into amphibolite facies. The rocks were affected by deformation in the later stages of arc development, going through a remelting process;
- Grayish-pink migmatized orthogneisses: represent rocks of granitic to granodioritic composition rich in quartz in stages of greater degree of melting;
- Porphyritic granodiorites and monzogranites: in this case, they are weakly deformed rocks rich in quartz diorite enclaves, with syn-plutonic dikes. They represent a moment of emplacement of the plutons linked to a phase of regional distension of the arc;
- High-K calcium-alkaline plutons: characterized by the emplacement of porphyritic or equigranular granodiorites, monzogranites and alkali-feldspar granitic composition. They appear after the formation of the arc and indicate the participation of crustal material.

URUBURETAMA GRANITIC SUITE

In the region of Itapipoca, Itapajé, Uruburetama, Irauçuba, Aracatiaçu Santa Quitéria and Tamboril, central-north of the state of Ceará (Fig. 1A), a series of granitic bodies of various dimensions (Uruburetama, Manoel Dias, Salgado, Extrema, Tapóra, Aracatiaçu, Tamboril granites, and several other smaller bodies) support a set of mountain ranges with maximum altitudes of the order of 1,000 m, the most significant one being the Uruburetama mountain. In the literature, this set of plutons is included in the Neoproterozoic TSQC, informally named "*Granitoides de Santa Quitéria*" (Cavalcante *et al.* 2003).

In the present work, the recognition of this set of granitoids is proposed under the denomination "*Uruburetama Granite Suite*", due to the several characteristics in common, taking as reference the most expressive body that supports the homonymous mountain (Uruburetama Batholith). The other bodies are defined in Figure 1, in the Geological Map of Ceará State and in the cartographic works of greater detail of the charts mapped by CPRM (Gorayeb *et al.* 2014, Naleto 2018, Braga 2017).

Geomorphologically, this unit forms residual dissection reliefs, in which forms of domed tops predominate, containing numerous valleys. As a curiosity, one of the main tourist symbols of the Itapajé region is the "*Pedra do Frade*", a natural geological monument that stands out in the Uruburetama massif, resembling the shape of a religious priest. Very common are the "*Pão de Açúcar*" like shapes, with large exposed boulders.

Geology and Petrography

Uruburetama Granite is a batholithic body of approximately 1,500 km^2 in area, with an elongated shape in the E–W direction (Figs. 1 and 2), inserted in the context of medium to high metamorphic gneissic terrains, where there is an intense migmatization process.

Country rocks are orthogneisses and aluminous paragneisses migmatized from TSQC. In addition, it is possible to observed biotite schists with garnet and sillimanite, marbles, calcium-silicate gneisses, quartzites, and amphibolite lenses, belonging to the Ceará Complex (Fig. 2) whose rocks establish diffuse contact relationships with transition to migmatites and, in rare cases, intrusive contacts with gneiss xenoliths.

The intrusive relationship is registered by the presence of xenoliths and mega-xenoliths of gneisses (Fig. 3A), with centimetric to decametric dimensions, with lenticular shapes, or ellipsoidal, circular, and elongated bodies (Fig. 3B). The borders of the xenoliths are, in general, well-defined with sharp contacts (Fig. 3C) and are also cut by apophysis and veins of the granite itself. The other relationship shows diffuse contacts with gradual transition to domains of migmatized gneisses, reaching the point of an intimate mixture between granites and gneisses with migmatitic features, indicating their generation by anatectic processes in high-grade metamorphic condition.

There is also the occurrence of cross dikes of mafic-dioritic composition, of metric dimensions, cutting the granitic rocks (Fig. 3D). The presence of elliptical or lenticular shaped enclaves is also frequent. One type is defined by concentrates rich in biotite, schlieren type (Figs. 3E and 3F) forming lenses or centimeter bands, oriented concurrently to foliation. Another type are the dioritic mesocratic rocks, medium grain size, which occur mixed with the granitic mass, generating rocks of hybrid composition probably related to the mixing of magmas. The presence of pegmatite veins of quartz-feldspar composition was also registered, dissecting the granitic rocks discordantly.

The UG has a variety of petrographic types that must correspond to a succession of magmatic pulses that vary compositionally from granodiorites to syenites. In the most central region of the body, the igneous character is recognized, and granitoids tend to be isotropic. Progressively moving away from the core of the body, the lithotypes exhibit foliations that are confused between magmatic (flow structure) or tectonic nature (mylonitic foliation). These structures, often both overlapping, reveal the coeval processes of emplacement of the bodies, cooling and deformation.

From petrographic studies, the Uruburetama granitic rocks were classified into six groups according to their mineralogical compositional affinities, textural similarities, and the intensity of the imposed deformation. Thus, the six classified petrographic facies are:

- biotite monzogranite;
- biotite syenogranite;
- biotite quartz monzonite;
- hornblende-biotite quartz syenite;
- biotite-hornblende granodiorite;
- leucomonzogranite.

The modal analysis was carried out on eight samples previously selected in order to represent the main types of rocks

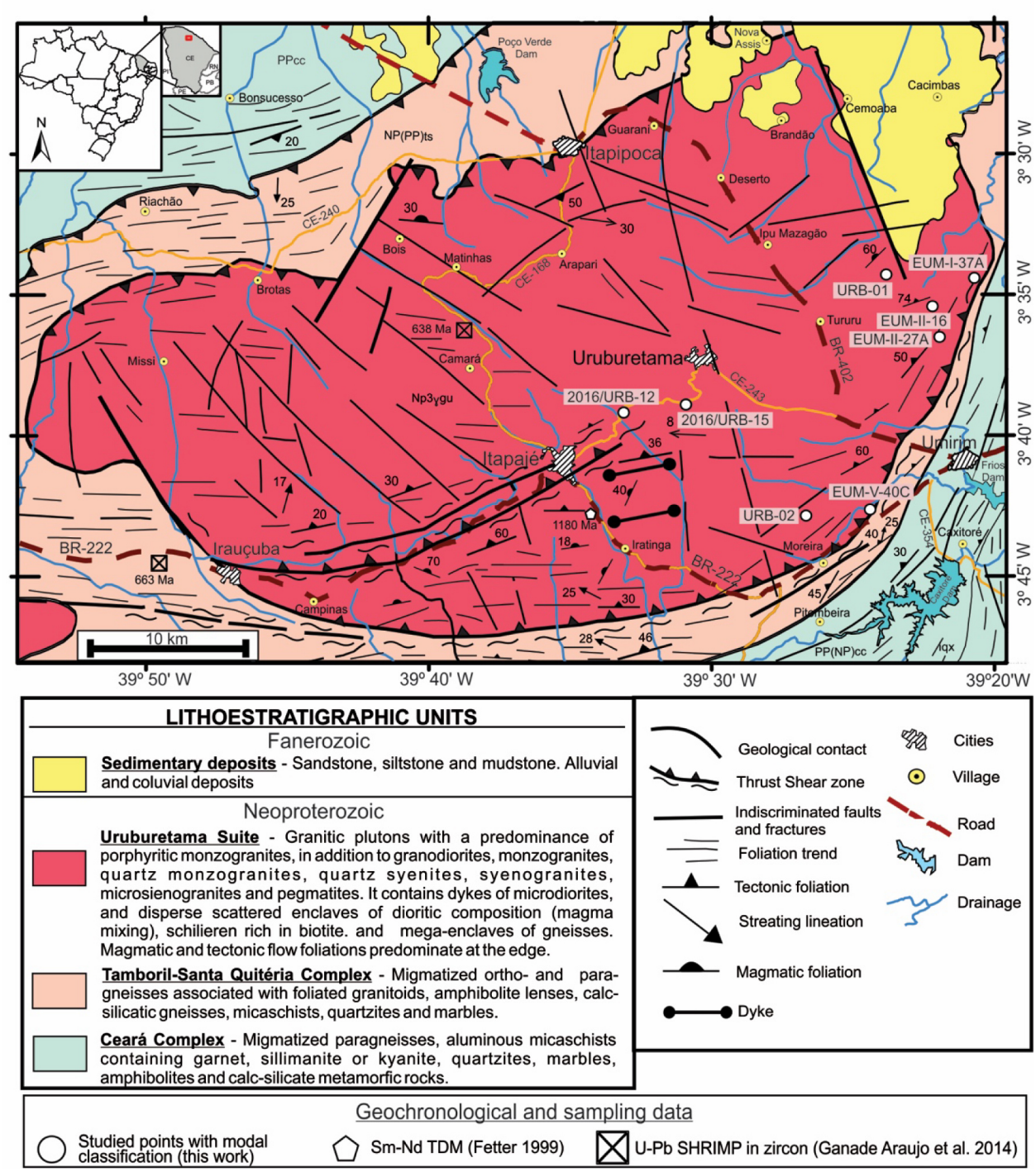

Figure 2. Geological map of Uruburetama Granite modified from the geological maps of the Ceará State (Cavalcante *et al.* 2003); SA.24-Y-D-V (Irauçuba sheets) (Naleto 2018), and data from this work.

of the UG (Tab. 1), and the results were plotted on the QAP diagram presented in Figure 4.

Petrographic typology

In this work, it was not possible to map the petrographic faciology of the batholith, due to the large size of the body, which would require more accurate work of aerogeophysical analysis, more extensive field work and petrographic studies with a sampling mesh more distributed throughout the body. The petrographic types will be described in more detail below and are summarized in Table 2.

Biotite monzogranite

This type represents the predominant petrographic facies in Uruburetama Granite, represented by monzogranitic rocks with biotite that may or may not contain hornblende (Tab. 2). These rocks can be found with two different structural characteristics: with weak to moderate deformation, which still preserve the igneous features as magmatic flow (Fig. 5A), or those strongly deformed and recrystallized (Meta-monzogranite) (Fig. 5B).

Overall, moderately deformed monzogranites have a light gray color with pinkish portions, are medium- or coarse-grained and have a leucocratic color index (M = 10–24).

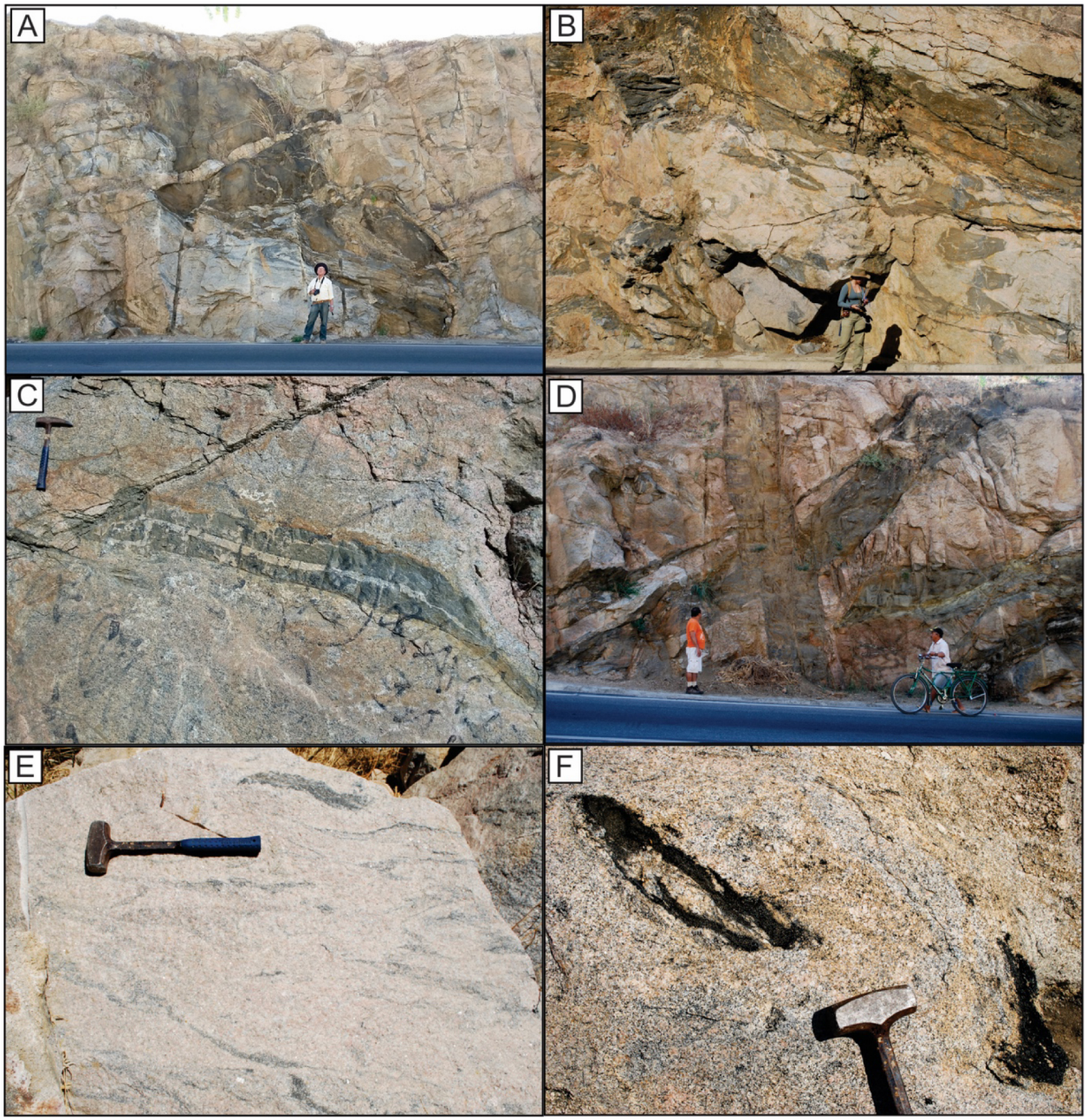

Figure 3. General aspects of the occurrence of granitoids, internal relations and contact of granitoids with country rocks: (A) Mega-enclave of gneiss injected by lenticular leucogranitic veins; (B) xenoliths of orthogneisses of different sizes and shapes in the granitic mass; (C) tabular bodies of angular metamorphic rocks and well-defined edges, following the granitoid foliation; (D) dikes of intercrossed meta-microdiorites, embedded in granitoid rocks; (E and F) biotite-rich enclaves defining schlieren-like structures, following the foliation of granitoid.

They are equigranular or porphyritic, with tabular crystals of euhedral microcline up to 6 cm. The phenocrystals show preferential orientation along with biotite and hornblende, composing the magmatic foliation, which is sometimes superimposed by the tectonic foliation. Relict structures can be observed such as, formation of mafic aggregates and plagioclase with oscillatory compositional zoning (Fig. 5C), hypidiomorphic granular texture (Fig. 5D), and quartz with slight undulating extinction.

In the most intensely deformed types, the mylonitic foliation predominates, which is well defined by the preferential orientation of biotite (Fig. 5E) and elongated porphyroclasts of microcline and ribbon quartz, characterizing the porphyroclastic texture (Fig. 5F). Microcline and plagioclase can also be found in the matrix with granoblastic texture. The formation of subgrains crowning the edges of porphyroclasts characterizes the mantle-core texture; intracrystalline microcracks are also observed (Fig. 5G). Quartz usually presents a strong wavy extinction and may be found as granular aggregates in triple-point contacts (granoblastic texture) or as stretched and ribbon crystals.

In these rocks, the occurrence of intergrowth simplectite features is frequent, the most common highlighting vermiform intergrowths of mimerkitic quartz at the edges of the plagioclase when in contact with alkali-feldspars. Similar features are recorded in biotite, when associated with hornblende

Table 1. Modal composition of Uruburetama Granite samples, in which 1200 points per sample were counted. Mineral abbreviations according to Fettes and Desmons (2007).

Minerais	EUM-V-40C	EUM-I-37A	EUM-II-16	EUM-II-27A	2012/URB-1	2012/URB-2	2016/URB-12	2016/URB-15
Qtz	25.0	19.1	24.4	17.9	25.4	18.9	33.2	13.8
Mc	34,.7	46.4	23.1	49.0	34.5	11.0	32.5	53.8
Pl	33.0	21.8	28.0	27.2	31.5	45.5	32.3	15.7
Bt	5.2	9.1	11.7	4.3	6.3	8.3	---	8.0
Msc	2.0	---	---	---	---	---	---	---
Hbl	---	---	10.6	---	---	11.0	---	5.6
Ttn	---	1.4	1.5	---	---	1.0	---	1.8
Zrn	---	---	0.1	0.1	0.1	0.2	0.1	0.4
Ap	---	0.1	---	---	---	0.1	---	0.2
Fl	---	---	---	---	0.4	2.3	1.1	0.2
Aln	---	0.2	---	---	0.4	0.2	---	---
Op	0.1	1.5	---	0.7	1.0	0.9	0.8	0.5
Total	100	99.6	99.4	99.2	99.6	99.4	100	100
Q	27	22	32	19	28	25	34	16
A	37	53	31	52	38	15	33	65
P	36	25	37	29	34	60	33	19
M	11.3	12.3	24.4	5.1	3	24	2	17

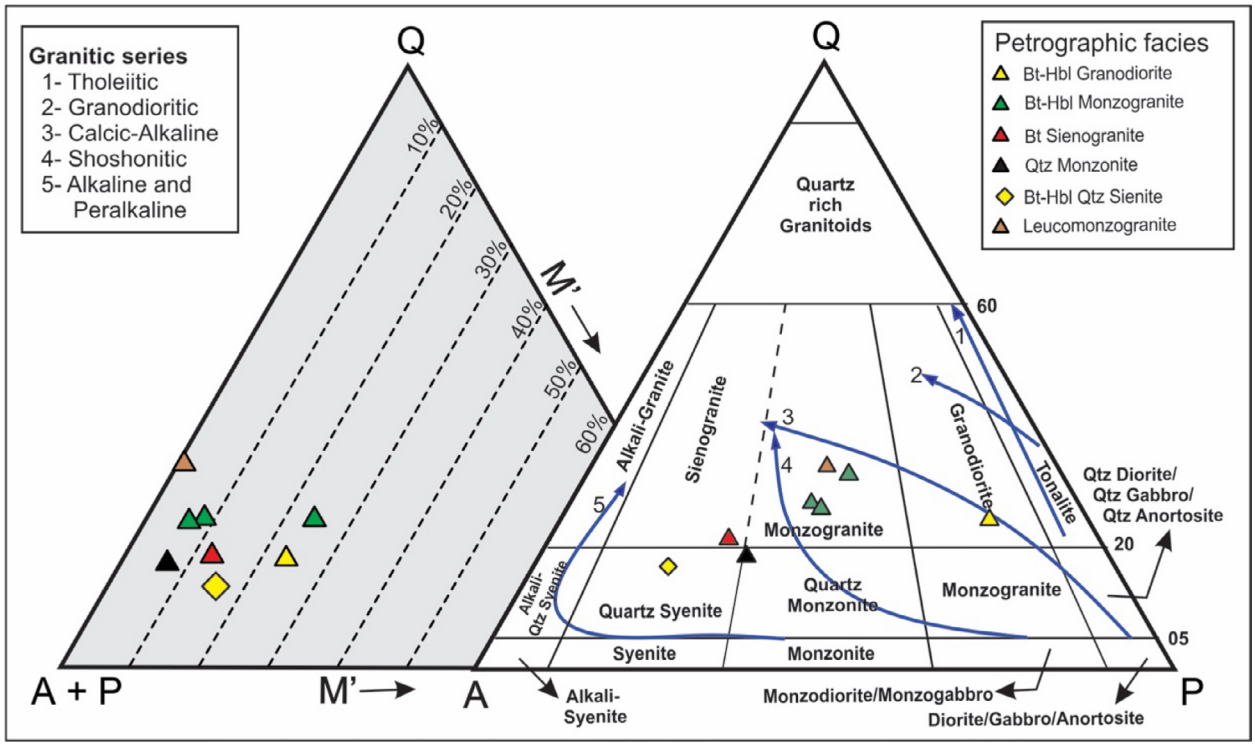

Figure 4. Quartz-alkalifeldspar-plagioclase (QAP) diagram of Streckeisen (1976) with the positioning of the petrographic types of the Uruburetama Granite samples.

in which vermiform features and microgranular quartz grow along the cleavages (Fig. 5H).

Biotite syenogranite

This petrographic facies is found in the southern portion of the batholith and at the northeast end of the study area. It emerges in large boulders on the slopes of the mountains or as extensive slabs. It is the second most abundant facies in the massif, with structural characteristics indicating incipient or well-defined deformation features (Figs. 6A and 6B). These are syenogranite rocks (Tab. 2) with pink color and whitish portions; they are medium- or coarse-grained

Table 2. Mineralogy and microstructural typology of the Uruburetama Granite petrographic types. Mineral abbreviations according to Fettes and Desmons (2007).

Facies	Mineral content		Color index (M)	Structure/Microestructure
	Essential	Accessory		
Biotite Monzogranite	Pl (30%) Mc (31%) Qtz (25%) Bt (5–12%) Hbl (8%)	Muscovite, Allanite, Fluorite, Zircon, Titanite, Opaque Min.	10–24	• Magmatic and tectonic foliation; • Porphyroclastic and granoblastic texture; • Ribbon Qtz; • Strong undulose extinction in Qtz; • Mantle-core texture; • Intracrystalline microcracks.
Biotite Syenogranite	Pl (22 %) Mc (47 %) Qtz (19%) Bt (8–10%)	Muscovite, Zircon, Titanite, Apatite, Allanite, Opaque Min.	5–12	• Magmatic and tectonic foliation; • Equigranular or porphyritic texture; • Bt+Ttn+Op aggregates; • Alignment of euhedral phenocrystals; • Mafic/intermediate enclaves; • Porphyroclastic and granoblastic texture; • Ribbon Qtz; • Mantle-core texture.
Hornblende-Biotite Quartz Syenite	Pl (16%) Mc (54%) Qtz (14%) Bt (8%) Hbl (6%)	Zircon, Titanite, Apatite, Allanite, Opaque Min.	8–16	• Magmatic foliation; • Porphyritic texture with hypidiomorphic granular in matrix; • Magma mingling; • Perthitic intergrowths in Mc; • Aggregates Bt + Hbl + Ttn + Op.
Biotite Quartz Monzonite	Pl (28%) Mc (50%) Qtz 18%) Bt (4%)	Zircon, Opaque Min.	5	• Tectonic foliation, • Porphyroclastic and granoblastic texture; • Mc and Qtz sub-grains with recrystallized edges.
Biotite-Hornblende Granodiorite	Pl (46%) Mc 11%) Qtz (20%) Bt (9%) Hbl (11%)	Fluorite, Zircon, Titanite, Allanite, Opaque Min.	21–25	• Tectonic foliation; • Porphyroclastic and granoblastic texture; • Weak undulating extinction in Microcline; • Mantle-core texture; • Intracrystalline microcracks.
Leucomonzogranite	Pl (32.3%) Mc (33%) Qtz (33.2%)	Zircon, Fluorite, Opaque Min.	1	• Isotropic structure; • Allotriomorphic granular texture; • Mimerkitic intergrowth.

and leucocratic (M = 5–12). They show equigranular or porphyritic general texture, in which the lithotypes least affected by the deformation and the alignment of euhedral alkali-feldspar phenocrystals characterize a magmatic flow feature; also, lentiform enclaves rich in mafic minerals follow the flow direction.

Under the microscope, they are characterized by the granoblastic texture composed of plagioclase, microcline, and quartz, sometimes in polygonal aggregates, with foliation marked by the preferred orientation of the biotite and locally with porphyroclastic texture (Figs. 6C and 6D).

Microcline occurs as almond-shaped porphyroclasts with sub-grain features and, together with biotite and plagioclase, they make up the rock matrix. Plagioclase is moderate to strongly saussuritized and some crystals exhibit normal oscillatory zoning. The granoblastic texture consists of granular aggregates of plagioclase, microcline, and quartz.

In the lithotypes more strongly affected by deformation, the general texture is porphyroclastic and locally granoblastic (plagioclase, microcline, and quartz; Fig. 6C), with mylonitic foliation marked by the preferred orientation of the biotite. Microcline porphyroclasts are the most common, while plagioclase, biotite, and quartz subgrains make up the rock matrix (Fig. 6D). Plagioclase is moderately to strongly saussuritized and some crystals exhibit normal oscillatory zoning.

In these rocks, biotite is the most abundant mafic mineral and occurs in two forms: as small crystals, less than 0.1 mm around the largest microcline crystals and defining the foliation of the rock (Fig. 6E); or as subhedral crystals in interstitial aggregates associated with opaque minerals and titanite, where in some portions they form random aggregates, on less deformed samples (Fig. 6F).

Hornblende-biotite quartz syenite

This petrographic type is found in a restricted way in the batholith, identified in small bodies in the central portion of the batholith. It is a leucocratic rock (M = 8–16, Tab. 2), porphyritic with subhedral or euhedral alkali-feldspar phenocrystals, from 1 to 2.5 cm grain size, immersed in a medium-grained hypidiomorphic granular matrix. Overall, the phenocrystals are preferably aligned, defining magmatic flow foliation (Figs. 7A and 7B), where there is little or no evidence of superimposed tectonic foliation. Also, evidence of magma mingling are found as fine-grained mafic enclaves with oval shapes (centimetric

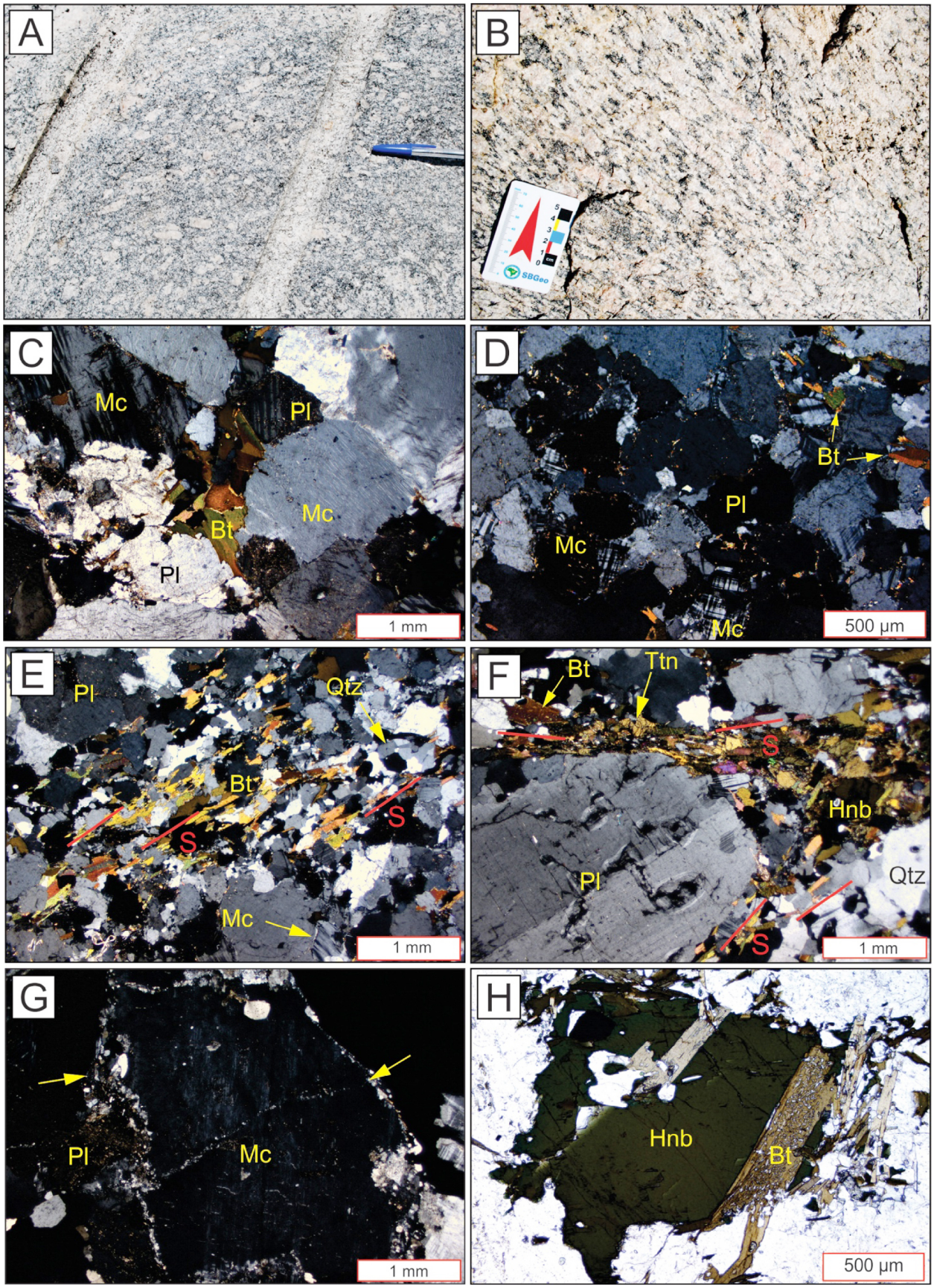

Figure 5. Structural features of Biotite-hornblende monzogranite: (A) structure of magmatic flow defined by euhedral crystals of alkali-feldspar preferably oriented; (B) mylonitic foliation highlighted by pinkish alkali-feldspar almonded porphyroclasts, ribbon quartz and biotite, preferably aligned; (C) concentrates of biotite and perthitic intergrowths in microcline; (D) hypidiomorphic granular texture defined by slightly elongated plagioclase and microcline; (E) tectonic foliation well defined by the preferred orientation of biotite; (F) deformed plagioclase porphyroclast, surrounded by mylonitic foliation enhanced by the orientation of biotite, hornblende and titanite; (G) deformed microcline porphyroclast with mantle-core texture and intracrystalline microcracks, indicated by the yellow arrows; (H) hornblende in parallel contact with biotite lamellar crystals. Note small vermiform and microgranular simplectites along the biotite cleavage. Mineral abbreviations according to Fettes and Desmons (2007).

to metric dimensions) containing xenocrystals of alkali feldspar, representing a mixture of magmas of extreme compositions (Fig. 7B).

The plagioclase occurs as subhedral or anhedral crystals, with moderate to strong alteration for sericite and epidote (Fig. 7C). The microcline predominantly presents subhedral or euhedral tabular phenocrystals with perthitic fillet-like intergrowths (Fig. 7D). Biotite, hornblende, and titanite occur in association, forming granular aggregates (Figs. 7E and 7F). Titanite commonly occurs as prismatic euhedral or subhedral forms, but also forms reaction crowns around opaque minerals (Fig. 7F). Granoblastic features are recorded in aggregates rich in microcline (Fig. 7G), and in certain cases highlighting foliation with preferential orientation of biotite and elongated quartz crystals (Fig. 7H).

Biotite quartz monzonite

This petrographic type was identified near the edges of the batholith, in the northeast portion and in the center-east part of the studied area. They are mineralogically similar to the Biotite monzogranite facies, differing by the lower percentages of quartz and color index (M ~ 5; Tab. 2).

The rocks have a light gray to pink color and are inequigranular medium-grained. The foliation is of mylonitic type,

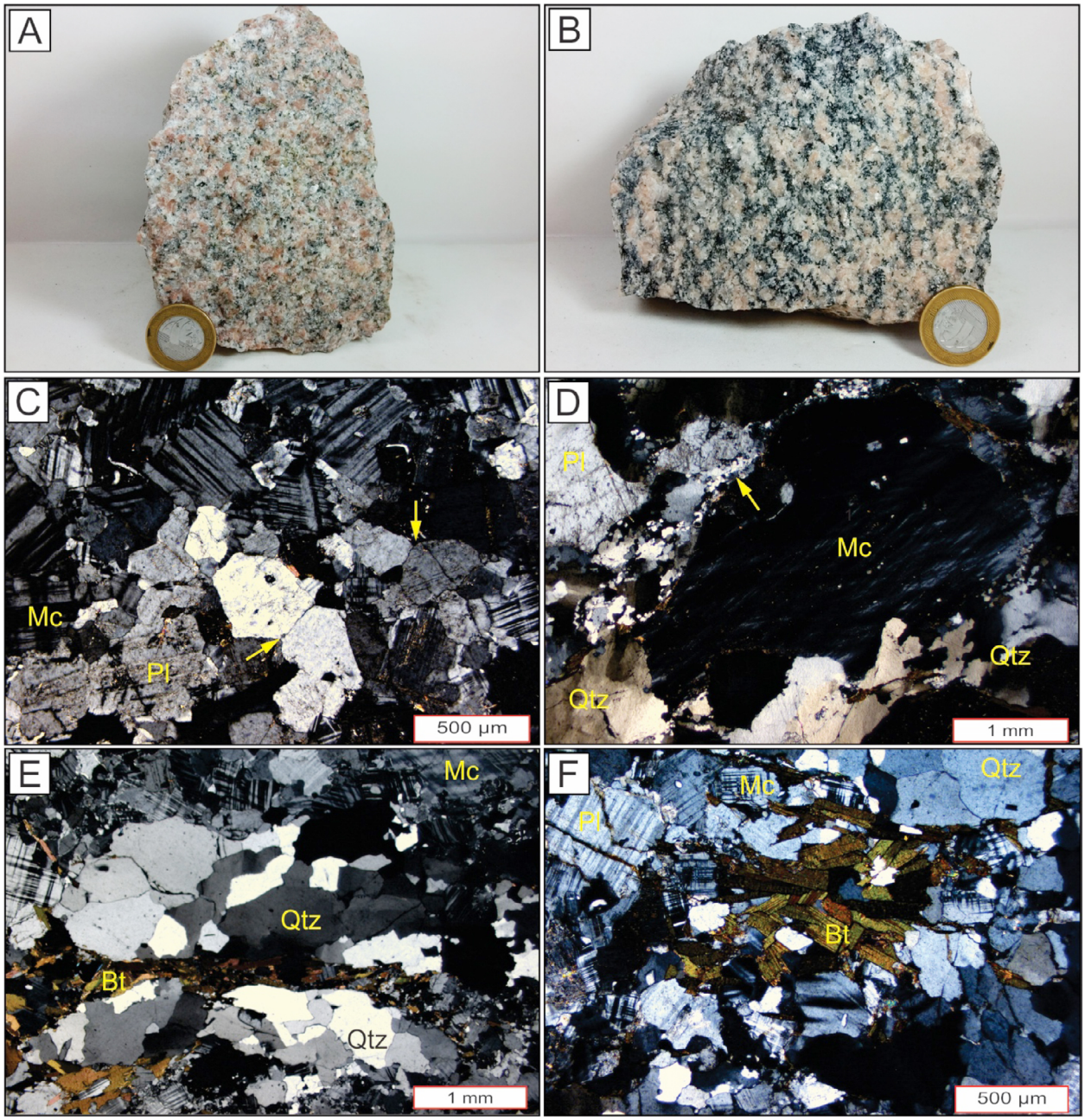

Figure 6. Textural/microstructural aspects of the Biotite Syenogranite facies: (A) hololeucocratic rock with isotropic character and medium-grained; (B) rock with pink color and dark brown tones, coarse-grained, higher color index and with foliation defined by the biotite orientation; (C) granoblastic texture with microcline and plagioclase crystals in triple point contacts; (D) elongated microcline porphyroclast with recrystallized edges, stretched quartz (ribbon) with subgrains and indented contacts; (E) stretched and recrystallized quartz, with foliation defined by oriented biotites (yellow traces); (F) random aggregates of biotite. All photomicrographs in crossed nicols (CN). Mineral abbreviations according to Fettes and Desmons (2007).

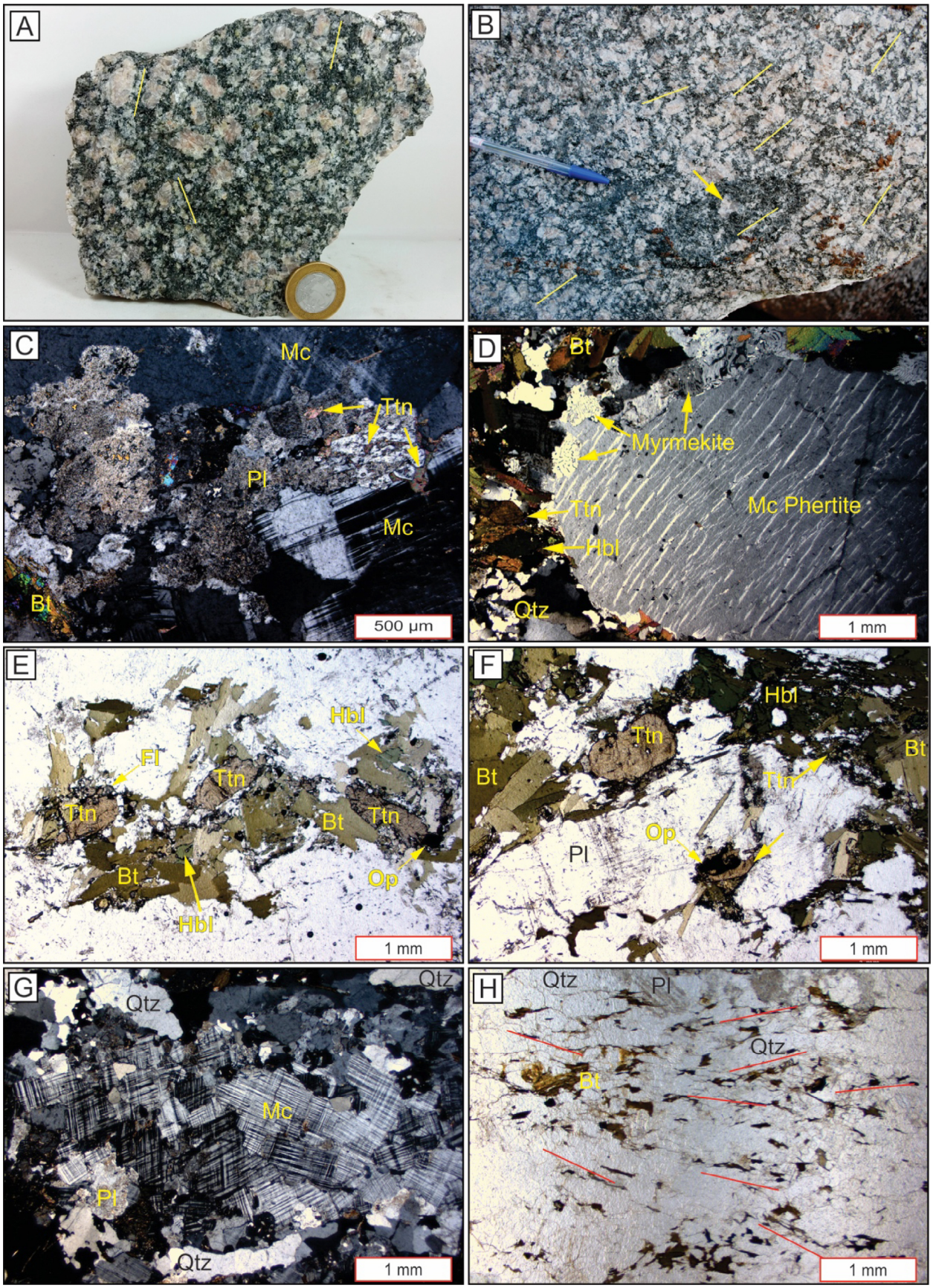

Figure 7. Petrographic features of Biotite Quartz Monzonite: (A) hand sample highlighting the porphyritic texture with alkali-feldspar phenocrystals; (B) oval mafic enclave with alkali feldspar xenocrystals following the alignment of the magmatic flow; (C) hipidiomorphic granular texture defined by aggregates of microcline, saussuritized plagioclase, quartz and titanite; (D) microcline phenocrystal with veinlet microperthitic intergrowth; (E, F) concentrate of mafic minerals with biotite, hornblende and titanite. Note coronitic titanite around the opaque mineral (yellow arrow); (G) granoblastic aggregate of microcline and quartz; (H) preferential orientation of biotite, enhancing foliation.C, D, G in crossed nicols (CN); E, F, G in natural light (NL). Mineral abbreviations according to Fettes and Desmons (2007).

highlighting the porphyroclastic texture, which follows the regional NEE–SWW trend, dipping 60–70° NW.

The rock is cut by pegmatite veins composed of quartz, alkali-feldspar, muscovite, and tourmaline. The presence of dioritic enclaves and biotite rich restites are recorded.

The microstructural features include mylonitic foliation (marked by the orientation of biotite, ribbon quartz, and some tabular feldspar crystals), polygonal fabric or subgrains of feldspars, forming the granoblastic texture (Fig. 7G). Biotite occurs around the microcline porphyroclasts, defining foliation (Fig. 7H).

Biotite-hornblende granodiorite

This petrographic type was found in the southeast portion of the batholith, they are dark gray, medium-grained, leucocratic (M = 21–24) rocks, which contained biotite and hornblende as main mafic phases (Tab. 2). They show porphyroclastic texture and well-defined tectonic foliation (Fig. 8A). Porphyroclasts are made of plagioclase, frequently strongly saussuritized (Fig. 8B), and alkali-feldspar in sizes between 0.5 and 2 cm.

The porphyroclastic texture is locally followed by granoblastic matrix (plagioclase, microcline, and quartz (Fig. 8C), but relict textures are recorded sporadically. The plagioclase and microcline porphyroclasts are oriented following the mylonitic foliation, with recrystallized edges in polygonal aggregates of fine grains characterizing the mantle-core texture (Fig. 8D). In general, these porphyroclasts, show micro cracks with undulose extinction, segmented and partially recrystallized (Fig. 8E).

Among the mafic minerals, hornblende is the most abundant one, occurring as prismatic, subhedral crystals or with very irregular shapes, presenting strong dark green (Z = Y) to pale yellow (X) pleochroism, defining foliation together with biotite (Fig. 8F).

Leucomonzogranite

This petrographic type is confined to the center-west portion of the study area. They are monzogranitic rocks with a whitish pink color, normally isotropic (Fig. 8G), medium-grained and medium highlighted by their hololeucocratic character (M = 1, Tab. 2), and are commonly cut by quartz-feldspar pegmatite veins. This facies has an allotriomorphic granular texture (Fig. 8H) and locally mimerkitic intergrowth, and shows no evidence of deformational processes. Taking into account the mineralogical composition and textural aspects, this facies is mainly composed of microcline, quartz and plagioclase, with fluorite, zircon and opaque minerals as accessories. Due to its extreme poverty in mafic minerals, textural aspects, and that it constitutes small bodies cutting the previous lithotypes, this petrographic type probably represents the most evolved rocks of the batholith, forming smaller bodies emplaced later in the magmatic evolution of UG.

TECTONO-STRUCTURAL FRAMEWORK AND METAMORPHISM

The overall structural picture of the CECD reveals a tectonic system of nappes with low dips foliations and stretching lineations that are related to the main tangential (collisional) tectonic phase. The deformation occurs progressively, and in the most evolved deformational increments, the crustal masses translated into large NNE-SSW dextral transcurrent shear zones, having Sobral-Cariré-Campo Lindo and Senador Pompeu zones as the main corridors for accommodating the deformation, which delimit the CECD; in addition to several other less significant shear zones, whose effects reached the whole set at the end of the Neoproterozoic (Arthaud and Torquato 1989, Gorayeb and Abreu 1989, Arthaud 2007, Ganade Araujo *et al*. 2014b).

In a more specific context, the deformation features are more prominent at the margins of the batholith, and in some internal portions, which are marked by shear zones with the development of mylonitic foliation with preferred orientation of biotite and amphibole, stretching lineation of quartz and feldspar that are elongated and recrystallized.

Magmatic flow foliation is also recorded, which is characterized by the alignment of subhedral crystals, especially tabular alkali-feldspar, and anhedral quartz.

These two types of structures are commonly confused in the outcrops, and specific criteria must be used to differentiate them, as established by Patterson *et al*. (1989) for the identification of tectonic and magmatic foliations in granitoids.

Magmatic foliation varies widely throughout the body, both in direction and in dipping. On the other hand, the tectonic foliation follows, approximately, the E-W trend in agreement with the gneissic banding of the country rocks, with a main direction of 80° Az and dips 30 to 40° NW.

A structural feature commonly present in the studied rocks, both in the body and in the country rocks, is the deformation of a mylonitic character, presenting itself as an anastomosed foliation that involves the lentiform feldspar porphyroclasts, the alignment of biotite and ribbon quartz, which is more prominent on the northern and southern flanks of the batholith where thrust and strike-slip shear zones were installed.

The regional structural framework of the northwest portion of the CECD records foliations with NNE-SSW directions, however, from the Aracatiaçu city, it presents a great inflection of the structures changing to E-W directions, in general with low to moderate dips (40°), for opposite quadrants, but, large folds modify this picture. However, along the contact of the plutons with the gneisses, the stretching lineation plunges gently to ENE and has a low rake indicating a dextral strike-slip movement. Boudinage features are recorded in alternating felsic bands with mafic portions or in neosomes in the orthogneisses.

In the structural context of the brittle regime, normal N–SW and NW–SE faults are frequent, and also a set of fractures, with three different families, in the NW–SE, NE–SW, and N–S directions.

Country rocks are migmatized gneisses of variable natures, in addition to other supracrustal rocks (garnet micaschists, quartzites, marbles, and calc-silicatic rocks). The orthogneisses are tonalitic to granodioritic in composition, gray in color, medium-grained, containing biotite and hornblende. They exhibit millimetric to centimetric gneissic banding, as well as centimetric

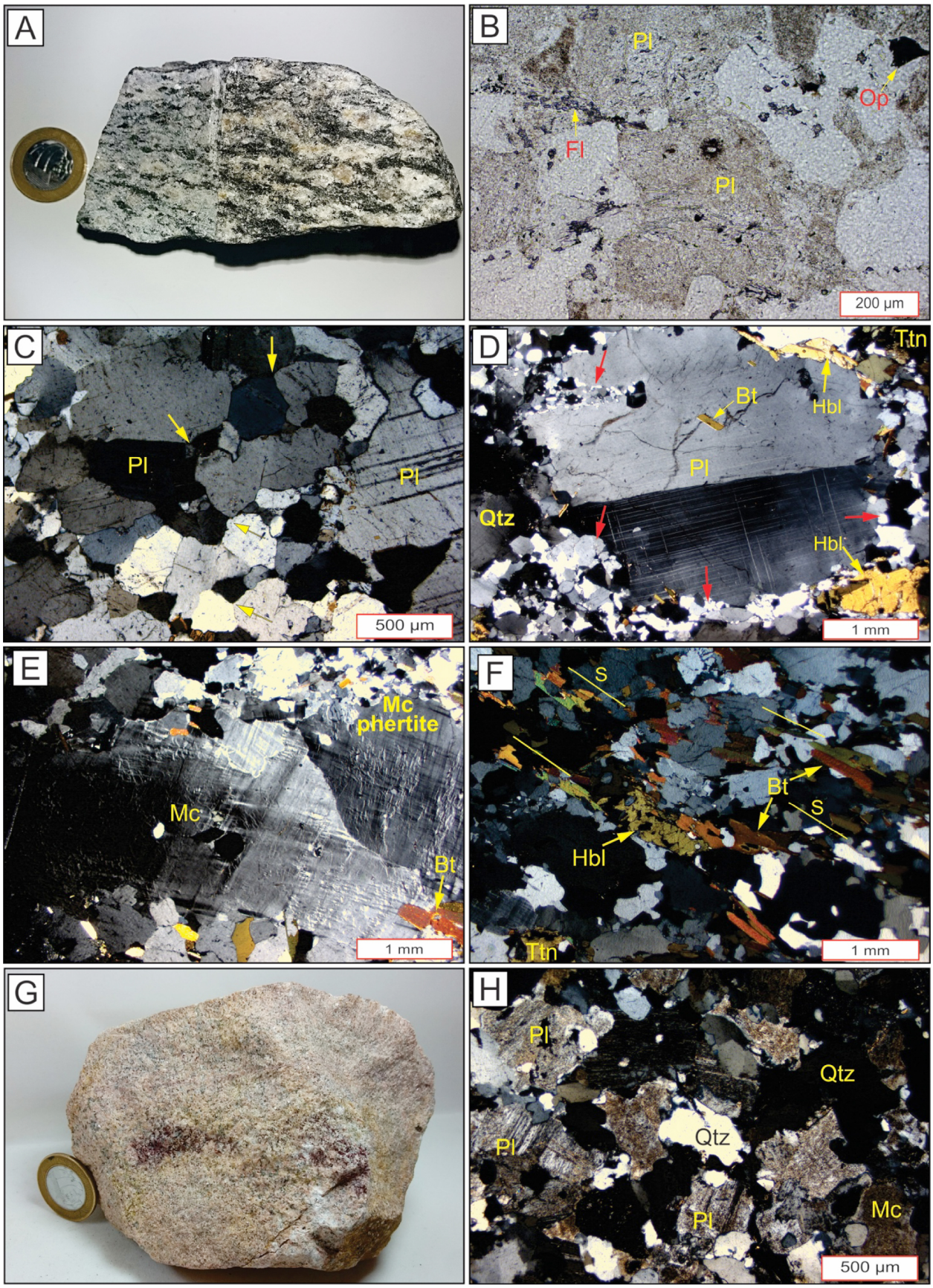

Figure 8. Photomicrographic aspects of the Biotite-hornblende granodiorite facies: (A) sample with well-defined orientation of biotite and hornblende and elongated feldspar crystals; (B) plagioclase crystals strongly saussuritized; (C) triple point framework of feldspar and quartz crystals defining the polygonal granoblastic texture; (D) plagioclase porphyroclast with recrystallized margins (red arrows) characterizing the mantle-core texture; note the deformation in the crystal with mechanical twinning, microcracks and bending of the twinning; (E) porphyroclast of perthitic microcline with recrystallization at the margins; note deformation with segmentation of the crystal, and strong ondulose extinction and bending of the twinning; (F) polygonal granoblastic texture with emphasis on foliation defined by biotite, hornblende, and titanite; (G) hand sample showing the hololeucocratic aspect of the rock; (H) allotriomorphic texture and isotropic character of the sample. All in crossed nicols (CN), except B. Mineral abbreviations according to Fettes and Desmons (2007).

shear bands. Migmatitic structures are variable, sometimes presenting discrete leucogranitic or pegmatitic, stromatic or networked neosomes, featuring metatexites according to Sawyer (2008) classification, but also diatexites with difficult separation between the migmatite parts.

Foliation follows the regional E–W trend with variation for NE-SW. Paragneisses and other supracrustal rocks show folded foliation with similar structural behavior. The presence of the Qtz + Bt + Grt + Sil ± Ky + Kfs paragenesis in the aluminous paragnaisses, and Di + Hbl ± Ca-Pl ± Grt ± Scp in calci-silicate gneisses, in addition to the extensive migmatization records in the adjacent terrain to the granitoid bodies allows to define metamorphic conditions in the high amphibolite facies to the region, reaching the anatexis isograde (moderate-high P and T > 680°C).

In addition, records of rocks formed in higher metamorphic conditions occurs in the units to the west of the SQMA, such as mafic and felsic granulites rich in garnet from the "Faixa de Alto Grau de Carire", associated with sin-transcurrent granitoids (Gorayeb and Abreu 1989); the Macaco Granulite unit in the Amontada region (Gorayeb and Abreu 1998) and the eclogitic slices in the Forquilha region (Ancelmi *et al.* 2013), all intensely reworked along the Sobral-Cariré-Campo Lindo Shear Zone (Fig. 1). These rocks represent segments of the lower crust tectonically exhumed in the region, which reveals the exposure of the roots of West Gondwana Orogen.

GEOCHRONOLOGY AND ISOTOPIC GEOCHEMISTRY

Analytical methods

Sample preparation and scanning electron microscopy

Two fresh rocks of the main lithotypes of the UG were sampled for age determination: one biotite monzogranite (URB-01) and one biotite-hornblende granodiorite (URB-02). Approximately 20 kg of a representative sample was crushed, ground, and sieved into fractions between 125 and 175 µm at Pará-Iso/UFPA.

For the whole-rock Sm-Nd isotope analyses, batches of two representative sample powders that had been previously prepared were used.

Zircon grains were separated using conventional heavy liquid (bromoform) and magnetic techniques. The zircon crystals are non-magnetic, exhibit bi-pyramidal, hexagonal euhedral prismatic, and length-to-width ratio between 2 × 1 to 5 × 1, yellow or caramel, transparent or translucent with marked concentric magmatic zoning (Fig. 9).

Representative zircon grains were handpicked under a binocular microscope (~100 grains/sample), mounted in epoxy resin discs and then polished to approximately half their thickness to expose the interior of the crystals. Prior to U-Pb dating, the internal structures of the zircon grains were examined using cathodoluminescence (CL) and backscattered electron (BSE) images obtained using a JEOL JXA-8230 scanning electron microscope (SEM) of the Microanalysis Laboratory/UFPA, working at 15 kV, 20 µA and a working distance of 11 mm. The acquired CL and BSE images were fundamental to observe the internal structure of the crystals (zoning, inclusions, and fractures) and to select the best areas for the specific isotopic analyses, as well as to direct, when possible, the laser beam in a same domain within the crystal for both U-Pb and Lu-Hf methodologies (Fig. 10).

For the Sm-Nd isotope analyzes, the samples were previously powdered following the techniques of Pará-Iso Lab. for chemical treatment.

Pb-evaporation/ionization zircon

The isotope analyses were carried out on a Finnigan MAT 262 thermo-ionization mass spectrometer (TIMS) at the Isotope Geology Laboratory, Universidade Federal do Pará

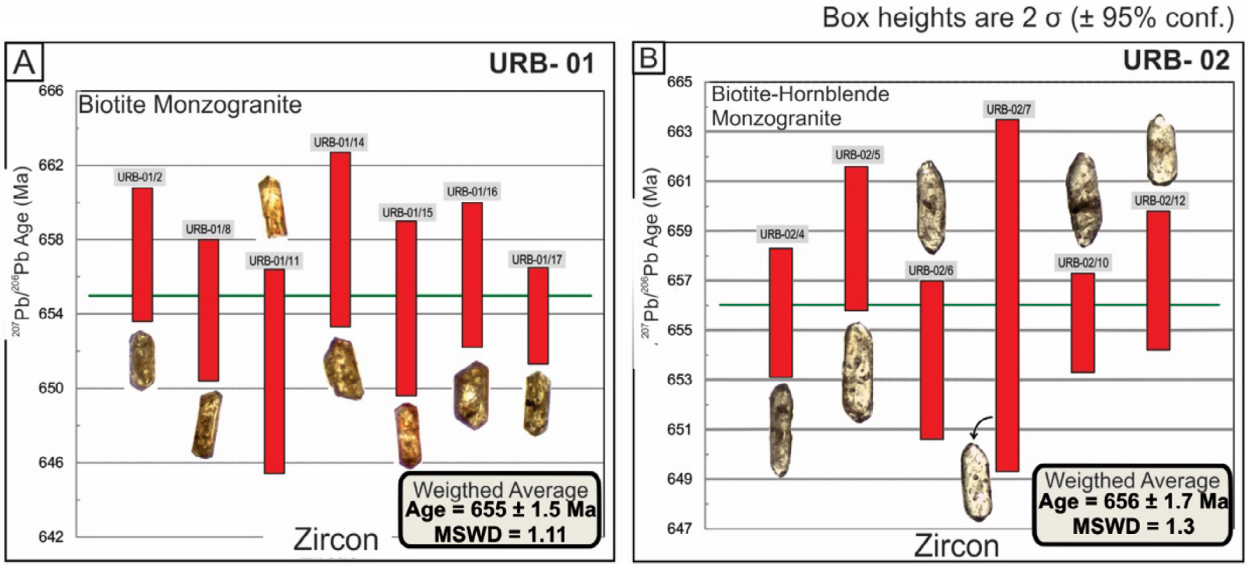

Figure 9. $^{207}Pb/^{206}Pb$ age (Ma) *versus* zircon diagrams for the (A) Biotite Monzogranite (URB-01) and Biotite-Hornblende Granodiorite (URB-02) samples from the Uruburetama Granite.

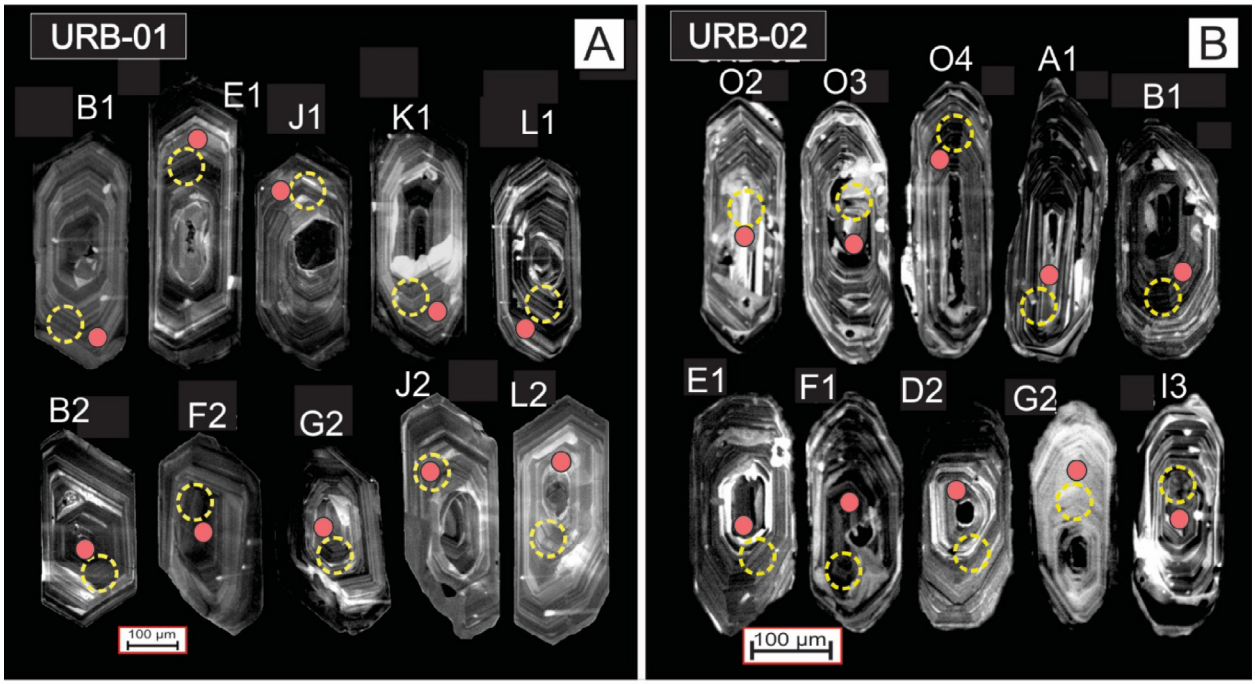

URB-01			URB-02		
Zircon	206Pb/238U (Ma)	$\varepsilon_{Hf(559)}$	Zircon	206Pb/238U (Ma)	$\varepsilon_{Hf(634)}$
B1	576 ± 26	-30.5	O2	690 ± 38	0.7
E1	554 ± 46	-30.5	O3	687 ± 26	0.3
J1	580 ± 26	-30.9	O4	662 ± 26	-0.3
K1	570 ± 27	-26.7	A1	653 ± 25	0.1
L1	572 ± 30	-32.0	B1	674 ± 24	1.1
B2	573 ± 29	-35.5	E1	640 ± 23	-0.4
F2	689 ± 25	-32,8	F1	628 ± 26	-1.5
G2	553 ± 25	-30.1	D2	610 ± 26	-1.0
J2	560 ± 25	-31.0	G2	629 ± 35	-2.0
L2	553 ± 23	-29.2	I3	630 ± 28	-2.1

Figure 10. Cathodoluminescence images of zircon crystals representative of URB-01 (A) and URB-02 (B) samples from Uruburetama Granite, with indication of the ages obtained individually. Red circles indicate the location of the U-Pb spots and yellow circles are Lu-Hf.

(Pará-Iso/UFPA), Belém-Brazil. For the Pb-evaporation method (Kober 1987), individual selected zircon grains were encapsulated in the Re-filament used for evaporation, which was placed directly in front of the ionization filament. The Pb is extracted by heating in three evaporation steps at temperatures of 1,450, 1,500, and 1,550°C and loaded into an ionization filament. Pb intensities were measured by each peak stepping through the 206–207–208–206–207–204 mass sequence for five mass scans, defining one data block with eight $^{207}Pb/^{206}Pb$ ratios. The $^{207}Pb/^{206}Pb$ weighted mean for each block is corrected for common Pb using appropriate age values derived from the two-stage model of Stacey and Kramer (1975), and results with $^{204}Pb/^{206}Pb$ ratios higher than 0.0004 and those that scatter more than two standard deviations from the average age value were discarded. The calculated age for a single zircon grain (Zircon software/Pará-Iso) and its error, according to Gaudette *et al.* (1998), is the weighted mean and standard error of the accepted blocks of data. Data were plotted in a diagram Age (Ma) *versus* zircon crystals analyzed with the Isoplot/Ex 3.2 (Ludwig 2003). The ages are presented with 2σ error.

Zircon U-Pb dating

LA-MC-ICP-MS zircon U-Pb analyses were carried out using a high-resolution multi collector Neptune Thermo Finnigan mass spectrometer coupled with a Nd:YAG LSX-213 G2 CETAC laser microprobe at the Pará-Iso/UFPA, whose instrumental performance and analytical procedures were documented by Chemale Jr. *et al.* (2012) and Milhomem Neto *et al.* (2017b). The laser-induced elemental fractionation and instrumental mass discrimination are corrected using the isotopic ratios of the homogeneous GJ-1 zircon (608.5 1.5 Ma; Jackson *et al.* 2004). For the correction of common lead contribution, the terrestrial Pb evolution model over time of Stacey and Kramer (1975) has been used. All corrections and raw

data reduction are processed using an in house Excel spreadsheet in order to calculate the corrected values of the isotopic ratios ($^{206}Pb/^{238}U$, $^{232}Th/^{238}U$, $^{207}Pb/^{206}Pb$) and uncertainties (1 sigma level in %). Age calculations and the presentation of isotopic results in the Concordia diagram are performed with the Isoplot/Ex 3.2 (Ludwig 2003). The strategy to define the most robust statistics and to determine the 'best' U-Pb age is that recommended by Spencer *et al.* (2016).

In situ zircon Lu–Hf isotopes

Zircon Lu–Hf isotope analyses were performed at the Pará-Iso/UFPA. The procedure of Hf analysis (Milhomem Neto *et al.* 2017a) was developed using a Neptune Thermo Finnigan multi collector MC-ICP-MS coupled with a Nd:YAG 213 nm LSX-213 G2 CETAC laser microprobe. The laser spot used was 50 μm in diameter with an ablation time of 60 s, repetition rate of 10 Hz, and He used as the carrier gas. Mass bias corrections of Lu-Hf isotopic ratios were done applying the variations of Mud Tank and GJ-1 standard. The raw data were processed in Microsoft Excel worksheets to calculate the $^{176}Hf/^{177}Hf$ and $^{176}Lu/^{177}Hf$ ratios, the Hf model-age and ε_{Hf} parameter for each analyzed point. ε_{Hf} has been calculated using current CHUR values of $^{176}Hf/^{177}Hf = 0.282785$ and $^{176}Lu/^{177}Hf = 0.0336$ from Bouvier *et al.* (2008). $^{176}Lu/^{177}Hf = 0.0388$ and $^{176}Hf/^{177}Hf = 0.28325$ were used for depleted mantle (Andersen *et al.* 2009). $^{176}Lu/^{177}Hf = 0.015$ were used as the average value for continental crust to calculate the two-stage crustal Hf model age ($Hf\text{-}T_{DM}^{C}$; Griffin *et al.* 2004, Belousova *et al.* 2010).

Whole-rock Sm-Nd isotopes

The analyses were conducted using a Thermo Finnigan Neptune multiple collector ICP-MS (MC-ICP-MS) with Faraday collectors at the Pará-Iso/UFPA. For each sample, ~100 mg of rock powder was weighed in a Teflon high-pressure vessel, mixed with a $^{150}Nd/^{149}Sm$ tracer solution and HF + HNO_3 acids, and reacted at 150°C, following the procedures described by Oliveira *et al.* (2008). After digestion, the solution was evaporated to dryness and then redissolved in HF + HNO_3 acids. This solution was then dried and taken up in 6N HCl, followed by sequential drying down and addition of 2N HCl. After evaporation, rare earth elements (REE) were isolated by chromatographic exchange using BioRad Dowex 50WX-8 cationic resin, 2N HCl and, 3N HNO_3. Sm and Nd were separated from the other REE and collected by passing the solution through a further set of ion exchange columns loaded with Dowex AGI-X4, 7N HNO_3 and, methanol. After evaporation, each separated Sm and Nd fraction was diluted with 1 ml HNO_3** (2%) and then analyzed by MC-ICP-MS. During this study, mass fractionation correction for $^{143}Nd/^{144}Nd$ was carried out relative to a $^{143}Nd/^{144}Nd$ of 0.7219 using the exponential law. The decay constant used was 6.54×10^{-12} $year^{-1}$ (Lugmair and Marti 1978) and chondritic values used to calculate ε_{Nd} were $^{143}Nd/^{144}Nd = 0.512638$ and $^{147}Sm/^{144}Nd = 0.1967$ (Ben Othman *et al.* 1984). Nd model ages ($Nd\text{-}T_{DM}$) for all the samples were calculated using the DePaolo (1981) model for a depleted mantle evolution. The La Jolla standard gave a mean $^{143}Nd/^{144}Nd$ value of 0.511834 ± 0.000005 (n = 6).

RESULTS

Zircon Pb-evaporation/ionization data

The analysis of the Biotite monzogranite (sample URB-01) was carried out on 17 zircon crystals, and the results (Tab. 3)

Table 3. Single-zircon Pb evaporation isotopic data for Biotite Monzogranite (URB-01) Biotite-Hornblende Granodiorite (URB-02) samples from the Uruburetama Granite.

Zircon	T (°C)	Ratios	$^{204}Pb/^{206}Pb$	± 2s	$(^{207}Pb/^{206}Pb)c$	± 2s	Age (Ma)	± 2s
Biotite monzogranite (URB-01)								
2	1,500	38/38	0.000167	0.000008	0.06151	0.00010	657.2	3.6
3	*1,580	0/32	0.000117	0.000025	0.12796	0.00023	2070.3	3.1
4	*1,550	0/34	0.000335	0.000007	0.06742	0.00043	850.9	13.2
5	#1,500	0/36	0.000442	0.000014	0.06868	0.00019	889.4	5.6
6	*1,500	0/32	0.000202	0.000003	0.06786	0.00028	864.6	8.6
7	*1,600	0/34	0.000142	0.000012	0.12317	0.00051	2002.9	7.3
8	1,500	36/36	0.000163	0.000007	0.06142	0.00011	654.2	3.8
9	*1,550	0/32	0.000233	0.000014	0.09158	0.00008	1459.0	1.7
11	1,550	32/40	0.000140	0.000006	0.06133	0.00016	650.9	5.5
12	#1,550	0/32	0.000464	0.000008	0.07052	0.00018	943.8	5.1
13	*1,550	0/32	0.000115	0.000006	0.08984	0.00054	1422.5	11.6
14	1,550	38/38	0.000199	0.000006	0.06153	0.00014	658.0	4.7
15	1,550	34/34	0.000152	0.000007	0.06142	0.00013	654.3	4.7
16	1,550	40/40	0.000173	0.000002	0.06147	0.00011	656.1	3.9
17	1,550	28/28	0.000125	0.000019	0.06141	0.00008	653.9	2.6
		254/518			**Weighted Average Age =**		**655.0**	**1.4**

Continue...

Table 3. Continuation.

Zircon	T (°C)	Ratios	$^{204}Pb/^{206}Pb$	± 2s	$(^{207}Pb/^{206}Pb)c$	± 2s	Age (Ma)	± 2s
Biotite-hornblende granodiorite (URB-02)								
1	*1,550	0/36	0.000089	0.000003	0.06438	0.00012	754.5	3.9
2	*1,550	0/40	0.000065	0.000032	0.06437	0.0002	754.0	6.5
3	*1,550	0/38	0.000066	0.000004	0.06445	0.00053	756.7	17.2
4	1,550	36/36	0.000102	0.000009	0.06146	0.00007	655.7	2.6
5	1,550	36/36	0.000158	0.000014	0.06155	0.00008	658.7	2.9
6	1,550	32/40	0.000165	0.000002	0.06141	0.00009	653.8	3.2
7	1,550	36/40	0.000160	0.000013	0.06148	0.00020	656.4	7.1
8	*1,550	0/34	0.000061	0.000005	0.06324	0.00022	716.7	7.3
9	*1,550	0/32	0.000042	0.000003	0.06367	0.00017	731.0	5.7
10	1,500	36/40	0.000126	0.000002	0.06145	0.00006	655.3	2.0
11	*1,550	0/40	0.000037	0.000005	0.06293	0.00022	706.3	7.5
12	1,550	38/40	0.000115	0.000002	0.06150	0.00008	657.0	2.8
		232/452				**Weighted Average Age =**	**656.0**	**1.7**

#Step not used due to scattering greater than two standard deviations from the average age; *step manually discarded due to higher or lower values of the $^{207}Pb/^{206}Pb$ ratio to the mean; c: ratios corrected for initial common.

of some crystals gave $^{207}Pb/^{206}Pb$ date values much higher than the average of the other crystals, as in the case of grains 3, 7, 9, 12, and 13, which presented age values ranging from 1.42 to 2.07 Ga, as well as crystals 1, 4, 5, 6, and 6, which were aged from 850 to 944 Ma. These crystals probably represent inherited grains. On the other hand, seven crystals showed analytically valid results for calculating age, using as a parameter the crystals whose ages overlapped, within their respective uncertainties, for the establishment of a plateau. According to these results, the determination of the average age value for the URB-01 sample of UG occurred in the stages of higher temperature. The $^{207}Pb/^{206}Pb$ ages considered valid were used to calculate a weighted mean age of 655 ± 1 Ma (n = 7, MSDW = 1.11, Fig. 9A).

The analysis in the Biotite-hornblende granodiorite (sample URB-02) was performed on 12 zircon crystals (Tab. 3). Among these, crystals 1, 2, 3, 8, 9, and 11 were excluded from the calculation because they have older $^{207}Pb/^{206}Pb$ dates ranging from 706 to 756 Ma, which exceeds the interval established as a parameter for defining the plateau in the diagram and possibly represent inherited crystals. In all, six crystals showed analytically valid results, according to the method, and were used in age calculation, taking as a parameter the crystals whose ages overlapped, within their respective uncertainties, for the establishment of the age. Among these, in grains number 4, 5, 6, 7, 10, and 12, the individual dates were the result of the analysis of the third evaporation stage (T = 1,550°C), with the other stages being eliminated sometimes by values above the average, sometimes by low quality of the analytical signal. According to these results, the $^{207}Pb/^{206}Pb$ dates considered valid were entered in an Age *versus* Zircon diagram and resulted in a $^{207}Pb/^{206}Pb$ weighted mean age of 656 ± 2 Ma (n=6, MSDW = 1.3, Fig. 9B).

U-Pb dating and Lu-Hf isotope data

U-Pb and Lu-Hf isotope data obtained on zircon grains, previously studied using CL and BSE images for the URB-01 and URB-02 samples (Figs. 10A and 10B), are listed in Tables 4, 5, and 6 and plotted in Concordia (Figs. 11 and 12) and $\varepsilon_{Hf}(t)$ *versus* age diagrams (Fig. 13). Among all analyzed points, those that presented significant common Pb contribution (high values of f_{206}) were not included in the isotope data table and, consequently, in the calculations of age. Likewise, discordant points with highly discrepant ages from the mean of each sample were discarded. U-Pb ages used for recalculation of Lu-Hf data are mean $^{206}Pb/^{238}Pb$ ages of truly concordant points. The 50 mm spots (Lu-Hf), when possible, were targeted near the U-Pb analytical point.

Twenty-eight URB-01 zircon crystals and twenty-nine URB-02 were analyzed by LA-MC-ICP-MS U-Pb, but in the URB-01 sample (Tab. 4) the crystal A1, D2, and H3, which presented age values ranging from 2.02 to 2.04 Ga, as well as crystals A2 and B5, which were aged from 656 to 704 Ma, probably represent inherited zircons. However, only 23 zircon crystal of URB-01 sample yielded concordant dates that defined a Concordia age of 559 ± 10 Ma (2σ, MSWD = 0.34) and a $^{206}Pb/^{238}U$ weighted average age of 559 ± 10 Ma (2σ, MSWD = 0.33, Fig. 11). While only 22 concordant zircon crystals of URB-02 sample defined a Concordia age of 634 ± 10 Ma (2σ, MSWD = 0.49) and a $^{206}Pb/^{238}U$ weighted average age of 635 ± 11 Ma (2σ, MSWD = 0.83, Fig. 12) with high degrees of concordance and analytical reliability, respectively. Thus, 634 Ma is interpreted as representing the crystallization age of UG. However, 559 Ma would represent a younger magmatic event, an age that was not confirmed by the Pb-Pb evaporation-ionization methodology.

Sample zircons (URB-01 and URB-02) were analyzed for Lu–Hf isotopes in domains with the same or similar internal structure as to those analyzed for U–Pb dating. In this study, all the Hf isotopic measurements were performed on zircons with more than 95% concordance on U-Pb ages. Initial $^{176}Hf/^{177}Hf$ ratios and $\varepsilon_{Hf}(t)$ values were calculated for the respective U-Pb age of crystallization of the granitoids. Ten representative zircons

Table 4. Zircon U-Pb isotope data obtained by LA-ICP-MS for Biotite Monzogranite (URB-01).

Spot	f_{206} [a] (%)	U ppm	Pb ppm	Th ppm	Th/U	$^{207}Pb/^{235}U$	1s (%)	$^{206}Pb/^{238}U$	1s (%)	Rho	$^{207}Pb/^{206}Pb$	1s (%)	$^{206}Pb/^{238}U$	1s abs	$^{207}Pb/^{235}U$	1s abs	$^{207}Pb/^{206}Pb$	1s abs	Conc. (%) 6/8–7/5
A1*	0.00	176	62	58	0.33	6.1421	13.1	0.3547	12.3	0.94	0.1256	4.3	1957	241	1996	437	2037	89	98
A1.2*	0.03	810	83	383	0.48	0.8574	7.0	0.1011	5.3	0.76	0.0615	4.5	621	33	629	103	656	30	99
B1	0.00	376	38	155	0.41	0.7599	5.9	0.0935	4.5	0.75	0.0590	3.9	576	26	574	46	565	22	100
E1	0.01	434	53	265	0.61	0.7255	9.3	0.0897	8.3	0.89	0.0587	4.2	554	46	554	64	555	23	100
J1	0.00	512	61	234	0.46	0.7594	5.5	0.0942	4.5	0.82	0.0585	3.2	580	26	574	41	548	17	101
K1	0.00	409	47	245	0.60	0.7388	5.8	0.0924	4.7	0.82	0.0580	3.3	570	27	562	43	529	17	101
L1	0.04	199	20	87	0.44	0.7587	6.6	0.0928	5.2	0.78	0.0593	4.1	572	30	573	51	579	24	100
B2	0.00	995	86	389	0.39	0.7422	6.3	0.0929	5.1	0.81	0.0579	3.8	573	29	564	46	527	20	102
D2*	0.04	233	91	57	0.25	6.1743	3.7	0.3572	3.0	0.80	0.1254	2.2	1969	58	2001	90	2034	45	98
F2	0.04	280	24	71	0.26	0.7823	5.8	0.0957	4.3	0.74	0.0593	3.9	589	25	587	44	578	23	100
G2	0.07	1,216	92	344	0.29	0.7294	4.6	0.0897	4.1	0.89	0.0590	2.1	553	23	556	33	567	12	100
J2	0.04	638	54	182	0.29	0.7413	5.1	0.0907	4.4	0.88	0.0593	2.4	560	25	563	37	578	14	99
L2	0.01	1,086	83	286	0.27	0.7362	4.7	0.0897	4.1	0.88	0.0596	2.2	553	23	560	34	587	13	99
B3	0.00	1,056	82	224	0.21	0.7113	5.1	0.0881	4.3	0.84	0.0586	2.8	544	23	546	39	551	15	100
D3	0.05	643	63	234	0.37	0.7067	5.1	0.0867	4.5	0.88	0.0591	2.4	536	24	543	36	570	14	99
E3	0.08	716	69	279	0.39	0.7328	5.6	0.0892	4.8	0.86	0.0596	2.9	551	26	558	43	589	17	99
H3*	0.05	340	129	89	0.26	5.6950	4.2	0.3326	3.5	0.83	0.1242	2.4	1851	65	1931	110	2017	48	96
L3	0.00	919	76	216	0.24	0.7228	5.0	0.0886	4.3	0.86	0.0592	2.6	547	23	552	36	573	15	99
B4	0.00	1,543	158	735	0.48	0.7263	5.3	0.0897	4.8	0.91	0.0587	2.2	554	27	554	37	557	12	100
E4	0.04	916	94	330	0.36	0.7347	5.4	0.0901	5.0	0.92	0.0592	2.1	556	28	559	37	573	12	99
H4	0.04	550	54	158	0.29	0.7407	5.9	0.0915	5.1	0.86	0.0587	3.0	564	29	563	44	557	17	100
J4	0.00	810	78	308	0.38	0.7074	5.5	0.0877	4.8	0.87	0.0585	2.7	542	26	543	41	549	15	100
B5*	0.09	1,425	135	454	0.32	0.8308	5.4	0.0958	3.3	0.61	0.0629	4.3	590	20	614	35	704	30	96
E5	0.04	2,007	198	666	0.33	0.7473	4.5	0.0914	3.9	0.85	0.0593	2.4	564	22	567	37	578	14	100
J5	0.00	973	110	421	0.44	0.7400	5.3	0.0916	4.5	0.85	0.0586	2.7	565	25	562	42	553	15	100
H6	0.03	739	64	186	0.25	0.7315	4.8	0.0897	4.2	0.87	0.0592	2.3	554	23	557	39	573	13	99
A7*	0.00	550	62	113	0.21	0.6617	10.5	0.0933	8.3	0.79	0.0515	6.3	575	48	516	69	261	17	111
D7	0.00	1,795	101	782	0.44	0.6921	5.3	0.0852	4.7	0.89	0.0589	2.4	527	25	534	39	563	14	99
G7	0.11	1,795	176	859	0.48	0.7497	5.1	0.0922	4.5	0.89	0.0590	2.3	568	26	568	39	567	13	100

[a]Fraction of the non-radiogenic ^{206}Pb in the analyzed zircon spot, where $f_{206} = [^{206}Pb/^{204}Pb]c / [^{206}Pb/^{204}Pb]s$ (c=common; s=sample); *zircons excluded from the calculation of age. LA-ICP-MS: inductively coupled plasma mass spectrometry.

Table 5. Zircon U-Pb isotope data obtained by LA-ICP-MS for Biotite-Hornblende Granodiorite (URB-02).

Spot	f_{206} [a] (%)	U ppm	Pb ppm	Th ppm	Th/U	$^{207}Pb/^{235}U$	1s (%)	$^{206}Pb/^{238}U$	1s (%)	Rho	$^{207}Pb/^{206}Pb$	1s (%)	$^{206}Pb/^{238}U$	1s abs	$^{207}Pb/^{235}U$	1s abs	$^{207}Pb/^{206}Pb$	1s abs	Conc.(%) 6/8-7/5
01*	0.03	73	10	35	0.48	0.9159	10.3	0.1150	5.8	0.57	0.0578	8.5	702	41	660	68	520	44	106
02	0.03	76	10	51	0.68	0.8538	8.8	0.1130	5.5	0.63	0.0548	6.8	690	38	627	55	404	28	110
03	0.04	168	23	103	0.62	0.9377	5.7	0.1124	3.8	0.66	0.0605	4.3	687	26	672	38	621	27	102
04	0.01	161	20	90	0.56	0.8794	5.7	0.1082	3.9	0.68	0.0589	4.1	662	26	641	36	565	23	103
A1	0.04	160	23	144	0.91	0.9003	6.2	0.1071	3.8	0.61	0.0610	4.9	656	25	652	40	638	31	101
B1	0.06	178	22	101	0.57	0.9204	5.0	0.1103	3.6	0.71	0.0605	3.6	674	24	663	33	623	22	102
D1*	0.00	68	11	43	0.63	1.1659	8.0	0.1407	5.9	0.73	0.0601	5.5	849	50	785	63	607	33	108
E1	0.00	214	22	64	0.30	0.8344	6.4	0.1043	3.5	0.55	0.0580	5.4	640	23	616	40	530	28	104
F1	0.03	174	22	148	0.86	0.8640	5.7	0.1024	4.2	0.74	0.0612	3.8	628	26	632	36	646	25	99
H1*	0.00	83	15	41	0.50	0.8656	16.5	0.1133	11.0	0.67	0.0554	12.3	692	76	633	105	429	53	109
I1*	0.01	44	7	74	1.72	0.7067	11.1	0.0965	6.6	0.59	0.0531	8.9	594	39	543	60	334	30	109
B2*	0.00	87	11	76	0.88	0.7590	10.2	0.1002	7.1	0.69	0.0550	7.3	615	43	573	58	410	30	107
D2	0.00	167	20	145	0.88	0.7790	6.0	0.0993	4.2	0.71	0.0569	4.3	610	26	585	35	488	21	104
G2	0.00	125	15	75	0.60	0.7955	7.8	0.1025	5.5	0.70	0.0563	5.6	629	35	594	47	464	26	106
H2*	0.02	98	13	61	0.63	1.0157	18.3	0.1214	16.7	0.91	0.0607	7.6	739	123	712	130	627	48	104
I2	0.06	112	22	206	1.85	0.8810	7.0	0.1050	4.8	0.67	0.0608	5.2	644	31	642	45	633	33	100
J2*	0.00	106	11	67	0.64	0.7497	10.3	0.1047	6.3	0.61	0.0519	8.2	642	40	568	58	282	23	113
H3	0.01	55	8	45	0.84	0.8541	9.7	0.1003	7.2	0.74	0.0618	6.5	616	44	627	61	667	44	98
I3	0.03	135	18	107	0.80	0.8793	6.4	0.1027	4.5	0.71	0.0621	4.5	630	28	641	41	678	30	98
C4	0.01	213	24	91	0.43	0.8385	6.1	0.1014	4.3	0.71	0.0600	4.3	623	27	618	38	602	26	101
D4	0.06	311	36	178	0.58	0.8530	4.9	0.1011	3.6	0.73	0.0612	3.4	621	22	626	31	646	22	99
E4	0.07	314	36	159	0.51	0.8588	4.7	0.1018	3.9	0.83	0.0612	2.6	625	24	629	30	646	17	99
H4	0.07	395	40	172	0.44	0.8514	5.0	0.1011	4.1	0.82	0.0611	2.8	621	25	625	31	641	18	99
J4	0.06	193	31	176	0.92	0.8743	4.4	0.1033	3.3	0.75	0.0614	2.9	634	21	638	28	653	19	99
C5	0.00	146	21	77	0.53	0.9195	6.9	0.1102	4.9	0.70	0.0605	4.9	674	33	662	46	621	31	102
E5	0.08	521	56	268	0.52	0.8599	7.3	0.1021	6.8	0.92	0.0611	2.8	627	42	630	46	643	18	99
G5	0.08	606	57	256	0.43	0.8352	4.2	0.0994	3.5	0.82	0.0609	2.5	611	21	617	26	637	16	99
H5	0.07	640	63	298	0.47	0.8427	3.9	0.1003	3.1	0.78	0.0610	2.4	616	19	621	24	638	16	99
B6	0.07	432	48	241	0.56	0.8461	4.6	0.1009	3.3	0.72	0.0608	3.2	620	20	622	28	633	20	100

[a]Fraction of the non-radiogenic ^{206}Pb in the analyzed zircon spot, where $f_{206} = [^{206}Pb/^{204}Pb]c / [^{206}Pb/^{204}Pb]s$ (c = common; s = sample); *zircons excluded from the calculation of age. LA-ICP-MS: inductively coupled plasma mass spectrometry.

Table 6. LA-ICP-MS Lu-Hf isotope data for zircon grains of Uruburetama Granite.

Spot	$^{176}Hf/^{177}Hf$	2SE	$^{176}Lu/^{177}Hf$	2SE	$\varepsilon_{Hf}(0)$	$t_{(U-Pb)}$ (Ma)	$(^{176}Hf/^{177}Hf)i$	$\varepsilon_{Hf}(t)$	T_{DM}^{C} (Ma)
Biotite Monzogranite (URB-01)									
B1	0.281584	0.000071	0.001189	0.000016	-42.47	559	0.281572	-30.48	3347
E1	0.281581	0.000058	0.000919	0.000011	-42.56	559	0.281572	-30.48	3346
J1	0.281573	0.000056	0.001202	0.000013	-42.88	559	0.281560	-30.89	3371
K1	0.281686	0.000072	0.000819	0.000021	-38.88	559	0.281677	-26.75	3121
L1	0.281537	0.000068	0.000684	0.000011	-44.14	559	0.281530	-31.97	3436
B2	0.281450	0.000077	0.001809	0.000028	-47.23	559	0.281431	-35.48	3647
F2	0.281516	0.000089	0.000872	0.000053	-44.88	559	0.281507	-32.78	3485
G2	0.281594	0.000087	0.001141	0.000066	-42.12	559	0.281582	-30.12	3325
J2	0.281569	0.000072	0.001084	0.000043	-43.02	559	0.281557	-30.99	3377
L2	0.281618	0.000069	0.000834	0.000027	-41.28	559	0.281609	-29.16	3266
Biotite-Hornblende Granodiorite (URB-02)									
02	0.282410	0.000048	0.000365	0.000018	-13.25	634	0.282406	0.74	1487
03	0.282399	0.000054	0.000450	0.000051	-13.66	634	0.282393	0.30	1515
04	0.282384	0.000077	0.000617	0.000057	-14.17	634	0.282377	-0.28	1551
A1	0.282401	0.000081	0.000971	0.000077	-13.59	634	0.282389	0.15	1524
B1	0.282422	0.000074	0.000600	0.000020	-12.82	634	0.282415	1.08	1466
E1	0.282379	0.000053	0.000494	0.000005	-14.34	634	0.282374	-0.40	1559
F1	0.282346	0.000063	0.000218	0.000025	-15.53	634	0.282343	-1.48	1626
D2	0.282362	0.000063	0.000443	0.000006	-14.95	634	0.282357	-0.99	1595
G2	0.282336	0.000077	0.000609	0.000008	-15.89	634	0.282328	-2.00	1659
I3	0.282336	0.000082	0.000766	0.000022	-15.89	634	0.282326	-2.07	1663

LA-ICP-MS: inductively coupled plasma mass spectrometry.

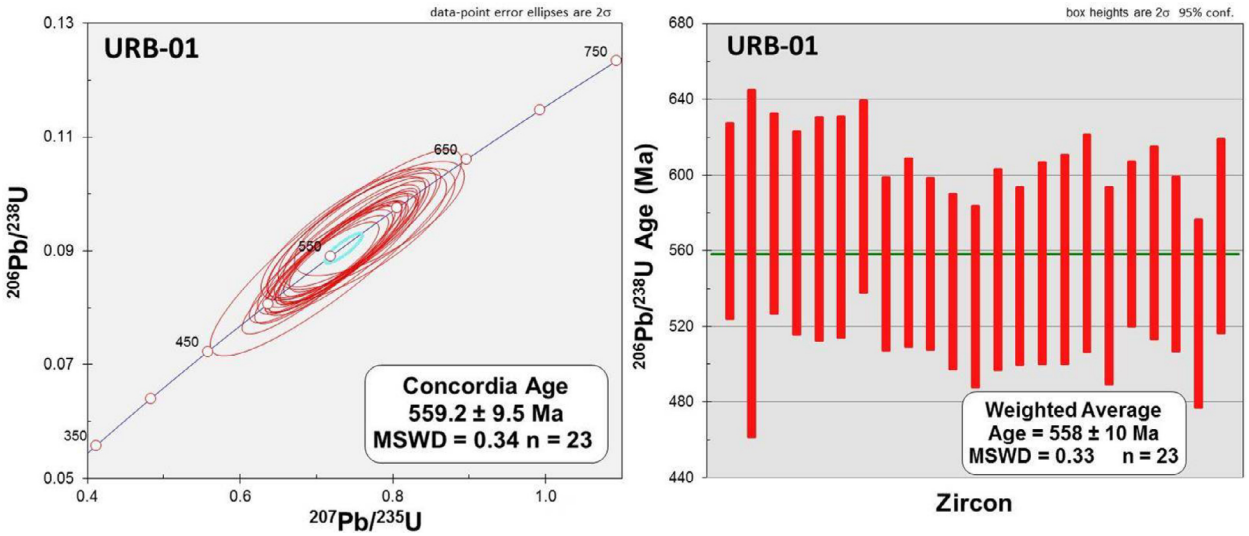

Figure 11. Inductively Coupled Plasma Mass Spectrometry (LA-ICP-MS) U-Pb concordia diagram and $^{206}Pb/^{238}U$ Age plot of the Biotite Monzogranite (URB-01).

of samples URB-01 and URB-02 were analyzed. The results for URB-01 show variable ε_{Hf} values ranging from -26.75 to -35.48 and Hf-T_{DM}^{C} model ages from 3,121 to 3,647 Ma with an average age of ~3.4 Ga (Tab. 6, Fig. 13). While the results for URB-02 show variable ε_{Hf} values ranging from -2.1 to +1.1 and Hf crustal model ages from 1,466 Ma to 1,663 Ma with an average age of ~1.6 Ga (Tab. 6, Fig. 13).

These data allow inferring two distinct episodes of crustal generation, one in the Meso-Eoarchean and the other in the Meso-Paleoproterozoic limit; the latter suggests a mixture

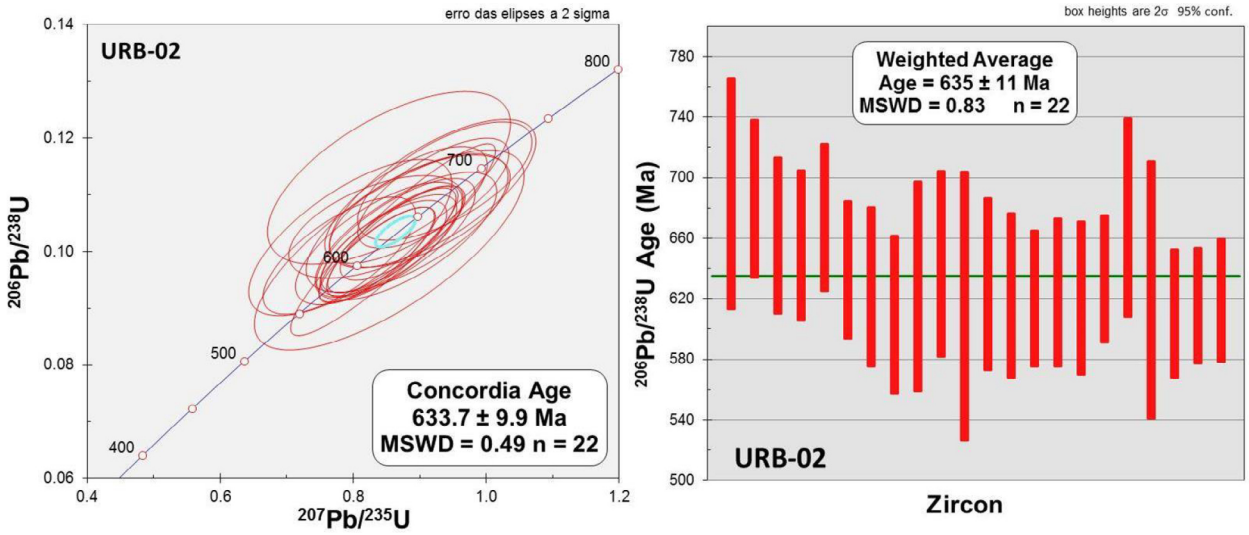

Figure 12. Inductively Coupled Plasma Mass Spectrometry (LA-ICP-MS) U-Pb Concordia diagram and $^{206}Pb/^{238}U$ Age plot of the Biotite-Hornblende Granodiorite (URB-02).

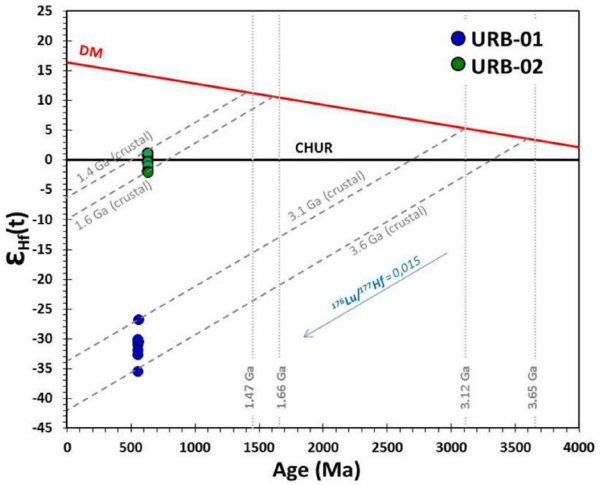

Figure 13. $\varepsilon_{Hf}(t)$ *versus* Age (Ma) evolution diagram for the Uruburetama Granite. The dotted lines represent crustal evolution trends, calculated using $^{176}Lu/^{177}Hf$ of 0.015 for the average continental crust (Griffin *et al.* 2004).

of juvenile Neoproterozoic source with Archean crustal contamination.

Sm-Nd whole-rock isotopes data

Whole-rock Sm-Nd data for Biotite monzogranite (URB-01) and Biotite-hornblende granodiorite (URB-02) samples are listed in Table 7 and plotted in an ε_{Nd} *vs.* Age (Ga) evolution diagram (Fig. 14). The $\varepsilon_{Nd}(t)$ values, calculated with the new U-Pb ages presented here, are predominantly negative, of -25.6 and -0.9. The Nd-T_{DM} model ages obtained show values of 2.9 (URB-02) and 1.2 Ga (URB-01). These data allow inferring two distinct sources of crustal generation, one in the Mesoarchean and another in the Mesoproterozoic. The Archean ages have a correspondence on the basement of the TSQC in the south of the CECD (Tróia Massif), and in São José do Campestre Massif (Fetter *et al.* 2000, Dantas *et al.* 1998). However, the Mesoproterozoic age is a problem to be discussed, because terrain with this type of age does not occur adjacent to BP. On the other hand, these age values can be interpreted as a mixture of sources, probably a juvenile neoproterozoic source with contamination of Archean crust.

DISCUSSION

Emplacement and magmatic evolution of the UG

Based on the geological data obtained in this study and in the literature, it is pertinent to discuss the emplacement and accommodation model of the UG, whose characteristics point to a sin-kinematic pattern. According to Neves (2012) and Gill (2009), the accommodation of contemporary tectonics bodies is shaped like elongated bodies with tectonic plots inside the plutons in agreement with those of the metamorphic country rocks, following the regional pattern. Contacts with country rocks are not abrupt; on the contrary, they are often gradual with migmatization involved, and with no thermal effects on the surrounding areas, but contemporary with regional metamorphism. All of these characteristics were identified in the UG, whose body shape corresponds to an elongated mega-almond (65 by 35 km), approximately E-W, in line with the regional trend of the gneisses.

There is no record of thermal metamorphic effects of the body on the adjacent rocks, featuring a low thermal gradient, and the contact of the granitoids with the enclosing gneisses is diffuse and gradual with an intimate mixture of granitic portions with migmatized gneisses, sometimes with mega-enclaves of gneisses near the edge of the granite. Internally, despite the records of preserved magmatic fabric (flow foliation with alignment of tabular feldspar phenocrystals) the tectonic fabric prevails, with striking mylonitic features, such as elongate feldspar porphyroclasts, ribbon quartz and preferentially oriented biotite lamellae. In addition, the structural framework of the area is marked by the low-angle tectonic foliation recorded

Table 7. Whole-rock Sm-Nd isotope data for granitoids from the Uruburetama Granite.

Sample	Sm (ppm)	Nd (ppm)	$^{147}Sm/^{144}Nd$	$^{143}Nd/^{144}Nd$ (± 2s)	$f_{(Sm/Nd)}$	$\varepsilon_{Nd}(0)$	$t_{(U-Pb)}$ (Ma)	$\varepsilon_{Nd}(t)$	Nd-T_{DM} (Ga)
URB-01	7.3	42.1	0.10473	0.510990 (18)	-0.47	-32.2	559	-25.6	2.9
URB-02	6.9	38.6	0.10846	0.512223 (10)	-0.45	-8.1	634	-0.9	1.2

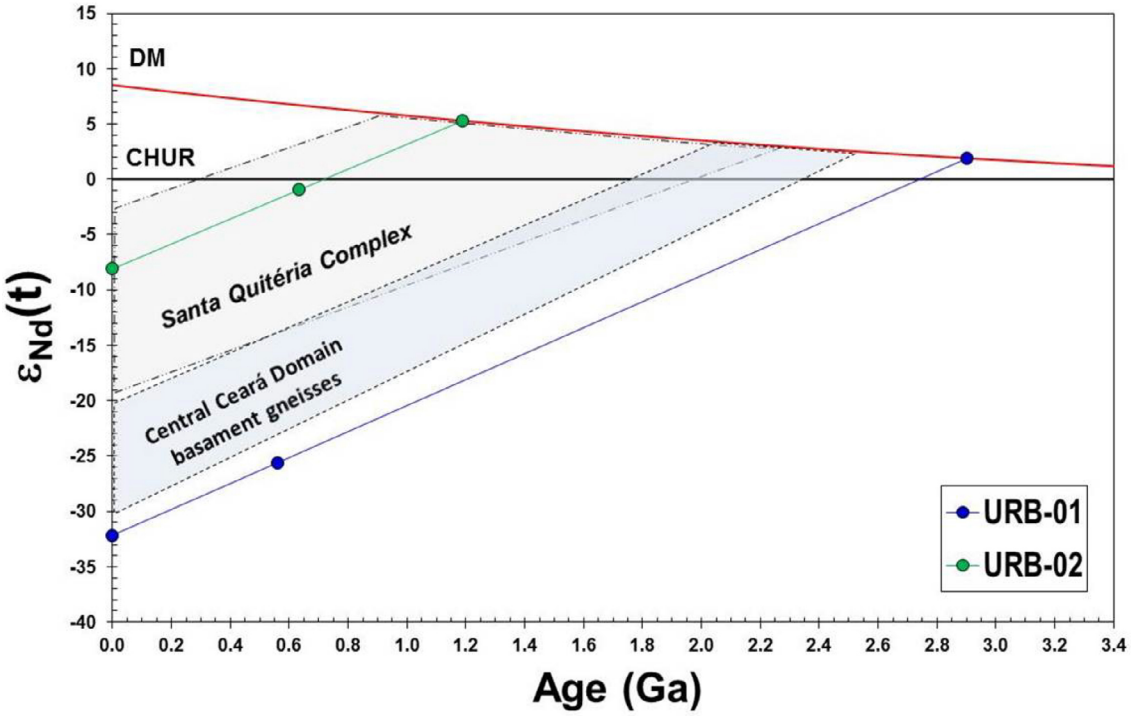

Figure 14. $\varepsilon_{Nd}(t)$ *versus* Age (Ga) diagram showing the evolution trends for the Uruburetama granite samples with delimitation of fields showing the evolution of the rocks of the Santa Quitéria Complex and gneisses of the basement of the Ceará Central Domain (Fetter *et al.* 2003).

on the granite flanks defining thrust zones, which confirms the emplacement of the granite simultaneously with the regionally tangential tectonics.

Because the UG is a very expressive body, the deformation was not high enough to reach the entire body, so that in some more internal portions of it, the igneous features are still preserved. This can also be explained by the multitemporal emplacement of the plutons. In this sense, the magmatic evolution of batholith is not simple, usually with multiple plutons emplacement, which is signaled by the different ages obtained in the bodies of the SQMA, and also by the contact relationships between the facies, internally, like the mafic-diorites dykes clearly housed in different stages. It is suggestive that some petrographic facies identified have evolved later, either due to processes of magmatic differentiation or by magmatic generations due to reflections in the evolution of the arc.

When analyzing the Streckeisen diagram (Fig. 4), it can be seen that granitoids exhibit a compositional variation with a certain trend, from granodioritic compositions to quartz syenitic, accompanied by variations in the color index, in addition to the dioritic bodies. Although there are no geochemical analyzes, this allows us to infer an increase in the silica and alkalis content, and a reduction in the Fe, Ca, and Mg content, suggestive of the performance of magmatic differentiation processes in the evolution of the batholith.

On the other hand, there is no doubt about the leucomonzogranite facies representing a more evolved magmatic phase, of late emplacement, as they form smaller dyke-like, finer-grained bodies.

One of the types of the enclaves forms irregular bodies of dioritic composition with xenocrystals of alkali-feldspar, and represent evidence of the magmas interaction of extreme compositions (magma mixing), probably generated in crustal melting (granitic) and material from the mantle (mafic).

In certain cases, mafic material appears as dikes cross cutting the granitic rocks. In others, the dykes are broken, showing diffuse contacts with the granitic rocks, in which the two magmatic phases are clearly mixed, revealing the contemporary positioning of magmas (magma mingling). In addition, schlieren-like enclaves, concentrated in biotite, must represent residues from anatexis of gneisses mixed in granitic masses.

From the textural analysis and post-magmatic reactions, it is possible to say that there were at least two moments of crystallization of the UG. The first was marked by the formation of monzogranites and granodiorites at a deeper crustal level during the period of residence of the magma in the magmatic

chamber, followed by deformation and metamorphism, in an anatexis setting. Dioritic bodies had their accommodation in continuity with the main crystallization of the batholith, sometimes marking clearly intrusive contacts and sometimes in magma mixing relationships featuring syn-plutonic dykes, possibly representing material from the lower crust or mantle.

Another stage marks the crystallization of more felsic phases, some of which cut the previous rocks in a moment of cooling the batholith tectonically transported to shallower crustal levels.

The formation of secondary mineral phases marks the beginning of the late-magmatic stage, which results from the percolation of late fluids with the participation of volatiles. This process leads to the decalcification of plagioclase (saussuritization), formation of fluorite and chlorite and formation of pegmatites.

In the evolutionary sequence, tectono-metamorphic processes imposed deformational fabrics related to the shear caused by the tangential tectonics that affected most of the batholith rocks, heterogeneously. Thus, mineral stretches are recorded, with emphasis on feldspar porphyroclasts, partly inherited from porphyritic textures, ribbon quartz, mylonitic foliations, and a variety of microstructures (mantle and core, sub-grains, triple point aggregates, crystal segmentation, mechanical twinning, boudinage).

Such features reveal the textures of metamorphic origin, in some cases superimposed on the primary magmatic features, such as recrystallization of feldspars and quartz, new formation of biotite, titanite and quartz simplectites interspersed in plagioclase and biotite.

According to the literature (Arthaud 2007), the maximum conditions imposed on the rocks of the region reached high-grade metamorphism at high pressure, reaching regionally high amphibolite facies. This is corroborated in the area by the paragenesis Kfs + Qtz + Grt + Sil ± Ky + Bt in aluminous paragneisses, and Di + Hbl ± Ca-Pl ± Grt ± Scp + Ttn in calc-silicate ones, in addition to the widespread migmatization in the region, indicative of minimum temperatures of 680°C.

Crystalization ages

The geochronological studies of the UG carried out in the present work, based on Pb evaporation-ionization analyzes in zircon single crystals, allowed the ages of 655 ± 2 and 656 ± 1 Ma to be obtained for monzogranitic and granodioritic rocks, respectively. LA-MC-ICP-MS zircon U-Pb analyzes for the same samples provided ages of 559 ± 10 and 634 ± 10 Ma. The general characteristic of zircon crystals with perfect shapes and peculiar oscillatory zoning reveal their magmatic origin, allowing interpreting these ages as representative of the magmatic phases of UG crystallization. Thus, the age of 634 Ma is interpreted as representing the crystallization age of the UG. However, the age of 559 Ma would represent a younger magmatic event, an age that was not confirmed by the Pb evaporation-ionization methodology, due to its limitations. However, the age this facie must be directly related to the shear zone that marks a Post-collisional phase I for the UG.

Figure 15 presents a chart by Ganade Araujo (2014a) that orders the temporal distribution of magmatic and metamorphic processes related to the evolution of the western BP. Within this framework, the representative granitic plutons of the region (Uruburetama, Chaval, Anil, Quixeramobim, Meruoca, and Taperuaba) were positioned chronologically for a comparative view.

Figure 16 presents an evolutionary sketch highlighting the main tectonic and magmatic events in the northwest of

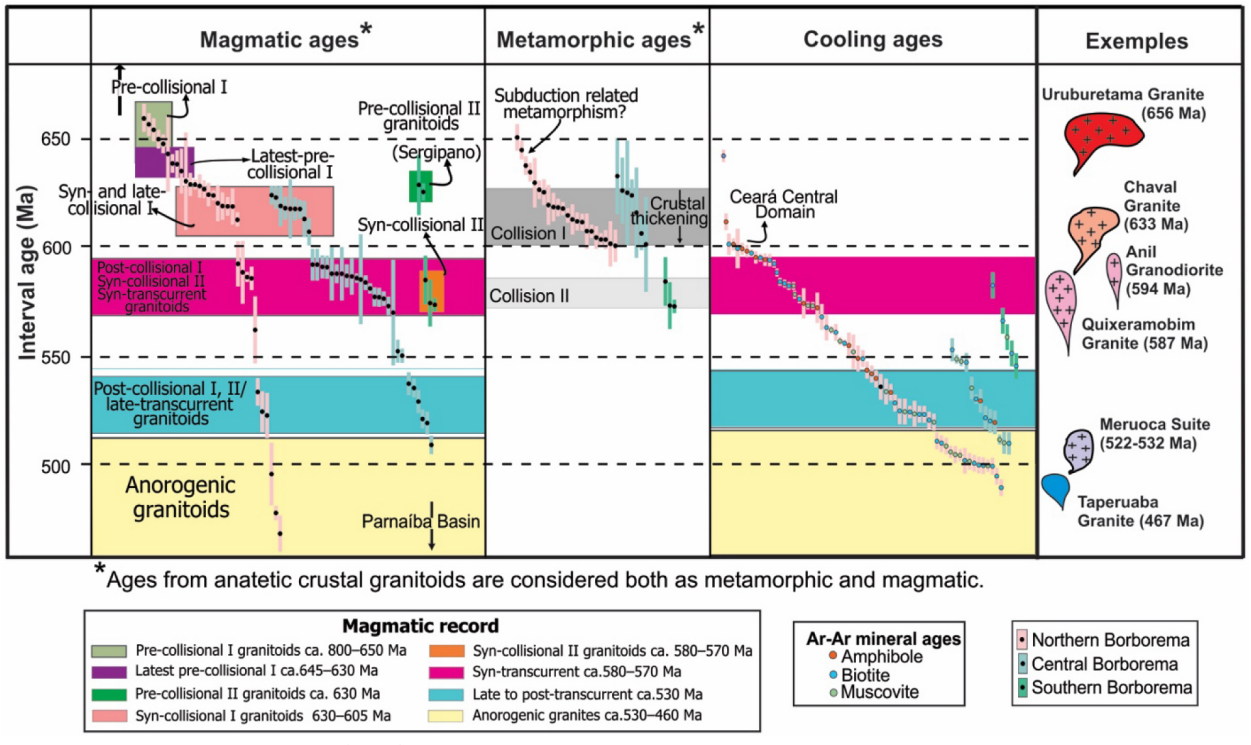

Source: adapted from Ganade Araujo *et al.* (2014a).

Figure 15. Scheme with the temporal distribution of magmatism and metamorphism related to the arc environment of granite rocks in the Borborema Province, with positioning of the Uruburetama Granite and some plutons representative of the various magmatic events in the region.

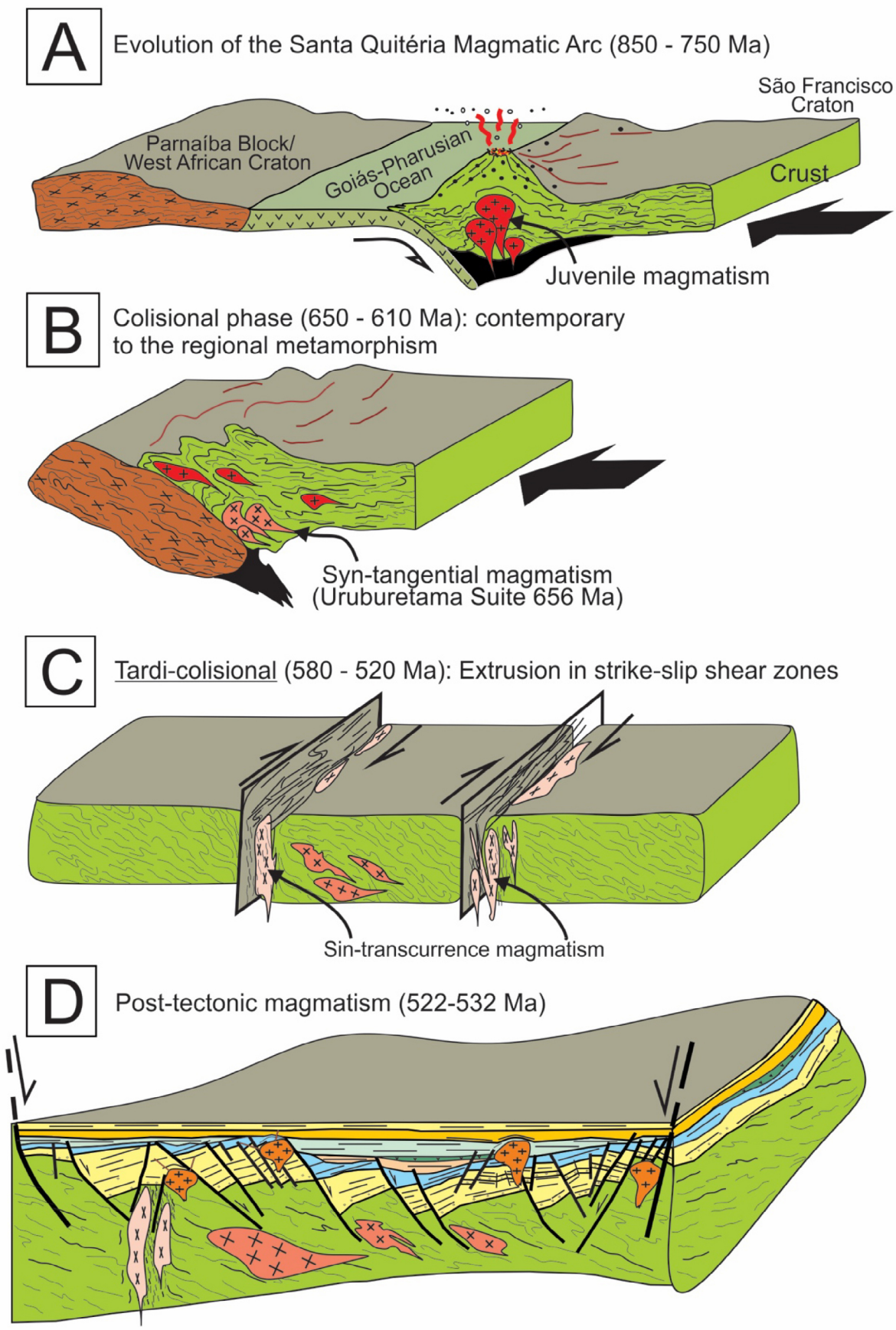

Figure 16. Evolutionary sketch to the northwest of Borborema Province with temporal positioning of granitoids in the tectonic stages of the SQMA, and the extensional tectonic end: (A) initial stage with establishment of the Goiás-Pharusian Ocean, subduction of the old oceanic lithosphere with generation of juvenile granitic magmatism (850–750 Ma); (B) configuration in a compressive setting, with regional high-grade metamorphism and deformation, crustal anatexis, and emplacement of sin-collisional granitoids (650–610 Ma); (C) final increments of the collisional tectonics with the lateral extrusion of crustal masses related to the development of strike-slip shear zones, and emplacement of sin-transcurrent granitoids (580–520 Ma); (D) extensional tectonics with the establishment of transtensional sedimentary basins (Ex. Jaibaras, Cococí, Jaguarapi, São Julião) accompanied by transitional-alkaline basaltic volcanism and accommodation of type A post-tectonic granites (*e.g.*, Meruoca Suite) (522–532 Ma).

BP, with an emphasis on the evolution of SQMA to post-tectonic magmatism related to the Eopaleozoic tectonics. The UG and associated plutons were emplaced in the main collisional phase of the evolution of the arc (650–610 Ma), (Fig. 16B) contemporary to the regional metamorphism. The youngest ages (~ 560 Ma) are related to the accommodation of late plutons that happened in the tardi-collisional phase of the orogen. In the advanced phase of the collision, other plutons were emplaced, now related to the development of transcurrent shear zones, and associated with the lateral extrusion of crustal masses (Fig. 16C). Other newer plutons of Ediacaran-Cambrian age were established during the extensional tectonics that led to the formation of rift basins with volcano-sedimentary filling (Fig. 16D), like the Jaibaras Graben.

Thus, we can position the main emplacement of the Uruburetama pluton in the Cryogenian, which coincides with that established for the beginning of the evolution of SQMA corresponding to the "Pre-Colisional I" or "Early-Sin-Orogenic" phase (Fetter *et al*. 2003, Ganade Araujo *et al*. 2014a), from a wide collisional belt in western BP.

Younger ages must represent granitoids related to the continuity of the orogen convergence of the Latest-Pre-collisional I (634 Ma) and Post-collisional I (559 Ma) phases, suggestive of multiple pluton emplacement.

Thus, we can conclude that the UG represents a voluminous body of granitic nature, with varied compositions, with records of a granitic plutonism event in the Cryogenian considered one of the most important representatives of the beginning of the evolution of SQMA associated with a large collisional belt named "West Gondwana Orogen" in the north of the BP.

Inherited zircons

The analytical results also reveal the presence of inherited zircons with values ranging from 2.0–2.1, 0.85–0.94, or 0.70–0.75 Ga. These data allow considering the contribution of different recognized units in the region. In the case of paleoproterozoic zircons, they would originate from the orthogneisses of the TSQC basement, such as the Forquilha Orthogneisse or units from the Tróia Massif. The other neoproterozoic age groups may represent zircons of granitoids from previous and early stages of the evolution of SQMA (Pre-collisional I, > 650 Ma) considering arc material recycling processes.

Sm-Nd and Lu-Hf T_{DM}

Sm-Nd and Lu-Hf isotopic data reveal the participation of older crustal sources in the generation of the UG. Sm-Nd whole-rock isotopes data indicate predominantly negative εNd(t) values and Nd-T_{DM} model ages of 2.90 and 1.2 Ga.

The results of Lu-Hf isotopes show negative ε_{Hf} values and Hf-T_{DMC} model ages of 3.12 to 3.65 Ga (URB-01) and 1.46 to 1.66 Ga (URB-02), allowing to infer two distinct crustal sources, Mesoarchean and Mesoproterozoic for the UG.

Zircon Hf crustal model ages and Sm-Nd T_{DM} of 2.9 and 3.6 Ga, evidencing that Archean crustal components contributed to the UG magma genesis. However, the mesoproterozoic ages are a problem to be solved, because terrain with this type of age does not occur adjacent to BP. The little-known Parnaíba Block would remain as a possibility of a Mesoproterozoic source, hidden beneath the sedimentary rocks of the Paleozoic Paraíba Basin. The Archean ages have representatives in the basement of SQMA at Tróia Massif and Granjeiro Complex.

CONCLUSION

UG constitutes a batholith of the most expressive and representative granitic body in the north of the CECD of BP, with great rocky exposure in the Uruburetama mountain. Considering that the UG is not an isolated pluton, and that there are several other granitic plutons with similar correlated characteristics (Patos, Manoel Dias, Extrema, Mirindiba, Aracatiaçu, Tamboril, and Nova Russas granites) distributed from south to north for more than 300 km, and in the literature are informally defined as "Santa Quitéria granitoids" here we are proposing the formalization of these granitoids occurrence as a new lithostratigraphic unit, named "Uruburetama Granitic Suite".

The Uruburetama batholith brings together a variety of plutonic and some sub-volcanic rocks, discriminating six petrographic facies, predominantly biotite-hornblende monzogranites and varieties of syenogranites, quartz monzonite, granodiorite, quartz syenite, and mafic-diorites rocks, and its metamorphic products, which represent different pulses in the magmatic evolution of the batholith.

The UG has several characteristics compatible with a model of sin-kinematic emplacement related to the collisional tectonics environment that took place at the CECD during the Brasiliano event in the Neoproterozoic.

The general characteristics of the studied rocks and zircon crystals, with perfect shapes and peculiar oscillatory zoning, reveal their magmatic origin. The zircon geochronological study showing ages of 656 Ma obtained for monzogranitic and granodioritic rocks are interpreted as indicators of the magmatic crystallization of zircon, and represent the main magmatic phases of crystallization of the UG. Younger ages (634 and 559 Ma) must represent generations of granitoids related to the continuity of the orogen convergence of the Latest-Pre-collisional I and Post-collisional I phases, respectively.

Inherited zircons showed three age groups (2.0–2.1, 0.85–0.94, and 0.70–0.75 Ga). In the case of paleoproterozoic zircons, they must have been assimilated from the orthogneisses of the Tamboril-Santa Quitéria Complex basement, such as the Forquilha Orthognaisse or Tróia Massif. The other Neoproterozoic age groups may represent zircons of granitoids from previous and early stages of the evolution of SQMA (Pre-collisional I, > 650 Ma) considering arc material recycling processes.

Zircon Hf crustal and Sm-Nd T_{DM} model ages of 2.9 to 3.6 Ga show an important Archean crustal component in the genesis of UG magma, and the possibilities would be the basement rocks of SQMA like the Tróia Massif and Granjeiro Complex. However, in the case of mesoproterozoic ages we could not find any corresponding rocks adjacent to BP, but this age can be interpreted as a mixture of sources — probably a juvenile Neoproterozoic one with Archean crustal

contamination. The little-known Parnaíba Block would remain as a possibility, hidden beneath the sedimentary rocks of the Paleozoic Paraíba Basin.

Finally, the UG represents a voluminous body of granitic nature and varied composition, with records of a granitic plutonism event in the Cryogenian (656 Ma), considered one of the most representatives of the beginning of the evolution of the SQMA associated with a large collision belt in the "West Gondwana Orogen" in the north of BP. The set of granites of the UGS are associated with gneissic-migmatitic terrains that have reached high-grade metamorphic conditions, in the anatexis zone, representing the exposure of lower crustal levels and the roots of this orogen.

ACKNOWLEDGMENTS

This study was conducted by the research group "Petrology and Crustal Evolution" of UFPA/CNPq, under the leadership of Prof. Dr. Paulo Gorayeb. The works were developed within the scope of the Faculty of Geology (FAGEO) and Geology and Geochemistry Graduate Program in Geosciences Institute of the Universidade Federal do Pará (PPGG/IG/UFPA). We are grateful to the Isotopic Geology Laboratory (Pará-Iso Lab) (IG/UFPA), where all the isotopic analyses were made and also to the Microanalysis Laboratory, where cathodoluninescence images were obtained. We also thank Prof. Dr. João Marinho Milhomem Neto for the critical review of topics related to the isotopic part.

ARTICLE INFORMATION

Manuscript ID: 20200034. Received on: 04/24/2020. Approved on: 08/03/2020.

P.S.S.G. acted as research advisor and coordinator, in the survey of field and sampling data; in the integration of data, text, discussion and interpretation of structural-tectonic and petrological topics; revised the article in its various versions; remade figures and rewrote discussion and conclusive topics; carried out the translation into English; L.C.S.S. acted in most stages of research development, from fieldwork to the preparation of the first version of the scientific article; prepared maps, figures, and tables; performed laboratory work, including petrographic analysis, sample preparation for geochronological studies; reviewed the advanced versions of the article; M.A.G. participated in obtaining, processing, calculating and interpreting geochronological data; wrote topics about Pb-Pb and U-Pb-Hf geochronology in zircon; in the elaboration and plotting of isotopic diagrams and in the general revision of texts, discussions, and interpretations.

Competing interests: The authors declare no competing interests.

REFERENCES

Almeida F.F.M., Hasui Y., Brito Neves B.B., Fuck R.A. 1981. Brazilian Structural Provinces: An Introduction. *Earth Science Reviews*, **17**(1-2):1-29. https://doi.org/10.1016/0012-8252(81)90003-9

Amaral W.S. 2010. *Análise geoquímica, geocronológica e geotermobarométrica das rochas de alto grau metamórfico, adjacentes ao Arco Magmático Santa Quitéria, NW da Província Borborema*. PhD thesis, Universidade Estadual de Campinas, Campinas, 234 p.

Amaral W.S., Santos T.J.S., Wernick E., Nogueira Neto J.A., Dantas E L., Matteini M. 2012. High-pressure granulites from Cariré, Borborema Province, NE Brazil: tectonic setting, metamorphic conditions and U-Pb, Lu-Hf and Sm-Nd geochronology. *Gondwana Research*, **22**(3-4):892-909. https://doi.org/10.1016/j.gr.2012.02.011

Ancelmi M.F., Santos T.J.S., Reginato R.A., Amaral W.S. Monteiro L.V.S. 2013. Geologia da Faixa Eclogítica de Forquilha, Domínio Ceará Central, noroeste da Província Borborema. *Brazilian Journal of Geology*, **43**(2):235-252. http://dx.doi.org/10.5327/Z2317-48892013000200004

Andersen T., Andersson U.B., Graham S., Åberg G., Simonsen S.L. 2009. Granitic magmatism by melting of juvenile continental crust: new constraints on the source of Paleoproterozoic granitoids in Fennoscandia from Hf isotopes in zircon. *Journal of the Geological Society*, **166**(2):233-248. https://doi.org/10.1144/0016-76492007-166

Aragão A.J.S., Gorayeb P.S.S., Galarza M.A. 2020. Magmatic and tectonic evolution of the Chaval Granite at the end of the Neoproterozoic, northwestern border of the Borborema Province. *Brazilian Journal of Geology*, **50**(1):1-26. https://doi.org/10.1590/2317-4889202020190089

Archanjo C.J., Launeau P., Hollanda M.H.B.M., Macedo J.W.P., Liu D. 2009. Scattering of magnetic fabrics in the Cambrian alkaline granite of Meruoca (Ceará state, northeastern Brazil). *International Journal of Earth Sciences*, **98**(8):1793-1807. http://dx.doi.org/10.1007/s00531-008-0342-z

Arthaud M.H. 2007. *Evolução neoproterozoica do Grupo Ceará (Domínio Ceará Central, NE Brasil): da sedimentação à colisão continental brasiliana*. PhD Thesis, Universidade de Brasília, Brasília, 132 p.

Arthaud M.H., Caby R., Fuck R.A., Dantas E.L., Parente C.V. 2008. Geology of the northern Borborema Province, NE Brazil and its correlation with Nigeria, NW Africa. *Geological Society, London, Special Publications*, **294**:49-67. https://doi.org/10.1144/SP294.4

Arthaud M.H., Fuck R.A., Caby R., Dantas E.L. Armstrong R., Garcia M.G. 2007. Evolução tectono-termal neoproterozoica (brasiliana) das nappes do Ceará Central, Borborema Setentrional (NE Brasil). *In*: Arthaud M.H. *Evolução neoproterozoica do Grupo Ceará (Domínio Ceará Central, NE, Brasil)*. PhD Thesis, Universidade de Brasília, Brasília, 132 p.

Arthaud M.H., Torquato J.R. 1989. A tectônica transcorrente no estado do Ceará. *In*: Simpósio Nacional de Estudos Tectônicos, 2., Fortaleza. *Annals*... SBG-NE. p. 77-278.

Belousova E.A., Kostitsyn Y.A., Griffin W.L., Begg G.C., O'Reilly S.Y., Pearson N.J. 2010. The growth of the continental crust: constraints from zircon Hf-isotope data. *Lithos*, **119**(3-4):457-466. https://doi.org/10.1016/j.lithos.2010.07.024

Ben Othman D., Polvé M., Allègre C.J. 1984. Nd-Sr isotopic composition of granulite and constraints on the evolution of the lower continental crust. *Nature*, **307**:510-515. https://doi.org/10.1038/307510a0

Bizzi L.A., Schobbenhaus C., Vidotti R.M., Gonçalves J.H. 2003. *Geologia, tectônica e recursos minerais do Brasil:* texto, mapas & SIG. Brasília: CPRM, 692 p.

Bouvier A., Vervoort J.D., Patchett P.J. 2008. The Lu-Hf and Sm-Nd isotopic composition of CHUR: constraints from unequilibrated chondrites and implication for the bulk composition of terrestrial planets. *Earth and Planetary Science Letters*, **273**(1-2):48-57. https://doi.org/10.1016/j.epsl.2008.06.010

Braga I.F. 2017. *Geologia e recursos minerais da Folha Ipueiras – SB.24-V-A-VI:* estados do Ceará e Piauí. Escala 1:100.000. 90 p.

Caby R, Arthaud M. 1986. Major Precambrian nappes of the Brazilian belt, Ceará, northeast Brazil. *Geology*, **14**(10):871-874. https://doi.org/10.1130/0091-7613(1986)14%3C871:MPNOTB%3E2.0.CO;2

Castro N.A. 2004. *Evolução geológica proterozoica da região entre Madalena e Taperuaba, domínio tectônico Ceará Central (Província Borborema)*. Doctoral thesis, Universidade de São Paulo, São Paulo.

Cavalcante J.C., Vasconcelos A.M., Medeiros M.F., Paiva I.P., Gomes F.E.M., Cavalcante S.N., Cavalcante J.E., Melo A.R.C., Duarte Neto V.C., Benevides H.C. 2003. *Mapa geológico do Estado do Ceará* – Escala 1:500.000. Fortaleza: CPRM.

Chayes F. 1956. *Petrographic modal analysis*. New York: John Willey & Sons, 113 p.

Chemale Jr. F., Kawashita K., Dussin I.V., Ávila J.N., Justino D., Bertotti A. 2012. U-Pb zircon in situ dating with LA-MC-ICP-MS using a mixed detector configuration. *Anais da Academia Brasileira de Ciências*, 84(2):275-296. https://doi.org/10.1590/S0001-37652012005000032

Costa F.G., Araújo C.E.G, Amaral W.S., Vasconcelos A.M., Rodrigues J.B. 2013. U-Pb (LA-ICPMS) zircon ages and Nd isotopes for granitoids of the Tamboril-Santa Quitéria Complex, Ceará Central Domain: Implication for Neoproterozoic syncollisional magmatism in north Borborema Province. *Geologia USP, Série Científica*, **13**(2):159-174. http://dx.doi.org/10.5327/Z1519-874X2013000200009

Costa F.G., Klein E.L., Lafon J.M., Milhomem Neto J.M., Galarza M.A., Rodrigues J.B., Naleto J.L.C., Lima R.G.C. 2018. Geochemistry and U–Pb–Hf zircon data for plutonic rocks of the Troia Massif, Borborema Province, NE Brazil: Evidence for reworking of Archean and juvenile Paleoproterozoic crust during Rhyacian accretionary and collisional tectonics. *Precambrian Research*, **311**:167-194. https://doi.org/10.1016/j.precamres.2018.04.008

Dantas E.L., Hackspacher P.C., Van Schmus W.R., Brito Neves B.B. 1998. Archean accretion in the São José do Campestre Massif, Borborema Province, Northeast Brazil. *Revista Brasileira de Geociências*, **28**(2):221-228. https://doi.org/10.25249/0375-7536.1998221228

DePaolo D.J. 1981. A neodymium and strontium isotopic study of the Mesozoic calc-alkaline granitic batholiths of the Sierra Nevada and Peninsular Ranges, California. *Journal of Geophysical Research*, **86**(B11):10470-10488. https://doi.org/10.1029/JB086iB11p10470

Fetter A.H. 1999. U-*Pb and Sm-Nd geochronological constraints on the crustal framework and geologic history of Ceará State, NW Borborema Province, NE Brazil: implications for the assembly of Gondwana*. PhD thesis, Department of Geology, Kansas University, Kansas, 164 p.

Fetter A.H, Santos T.J.S., Van Schmus W.R, Hackspacher P.C., Brito Neves B.B., Arthaud M.H., Nogueira Neto J.A.A., Wernick E. 2003. Evidence for neoproterozoic continental arc magmatism in the Santa Quitéria Batholith of Ceará State, NW Borborema Province, NE Brazil: implications for the assembly of West Gondwana. *Gondwana Research*, **6**(2):265-273. https://doi.org/10.1016/S1342-937X(05)70975-8

Fetter A.H, Van Schmus W.R, Santos T.J.S., Nogueira Neto J.A.A., Arthaud M.H. 2000. U-Pb and Sm-Nd geochronological constraints on the crustal evolution and basement architecture of Ceará State, NW Borborema Province, NE Brazil: implications for the existence of the Paleoproterozoic supercontinent "Atlantica". *Revista Brasileira de Geociências*, **30**(1):102-106.

Fettes D., Desmons J. 2007. *Metamorphic rocks:* classification and glossary of terms. Cambridge: Cambridge University Press, 244 p.

Ganade Araujo C.E., Cordani U.G., Basei M.A.S., Castro N.A.C., Sato K., Sproesser W.M. 2012a. U–Pb detrital zircon provenance of metasedimentary rocks from the Ceará Central and Médio Coreaú Domains, Borborema Province, NE-Brazil: Tectonic implications for a long-lived Neoproterozoic active continental margin. *Precambrian Research*, **206-207**:36-51. https://doi.org/10.1016/j.precamres.2012.02.021

Ganade Araujo C.E., Cordani U.G., Weinberg R.F., Basei M.A.S, Armstrong R., Sato K. 2014a. Tracing neoproterozoic subduction in the Borborema Province (NE-Brazil): Clues from U-Pb geochronology and Sr-Nd-Hf-O isotopes on granitoids and migmatites. *Lithos*, **202-203**:167-189. https://doi.org/10.1016/j.lithos.2014.05.015

Ganade Araujo C.E., Costa F.G, Pinéo T.R.G., Cavalcante J.C., Moura C.A.V. 2012b. Geochemistry and $^{207}Pb/^{206}Pb$ zircon ages of granitoids from the southern portion of the Tamboril-Santa Quitéria granitic-migmatitic complex, Ceará Central Domain, Borborema Province (NE-Brazil). *Journal of South American Earth Sciences*, **33**(1):21-33. https://doi.org/10.1016/j.jsames.2011.07.009

Ganade Araujo C.E., Weinberg R.F., Cordani U.G. 2014b. Extruding the Borborema Province (NE-Brazil): a two-stage neoproterozoic collision process. *Terra Nova*, **26**(2):157-168. https://doi.org/10.1111/ter.12084

Gaudette H.E., Lafon J.M., Macambira M.J.B., Moura C.V., Scheller T. 1998. Comparison of single filament Pb evaporation/ionization zircon ages with conventional U-Pb results: examples from Precambrian of Brazil. *Journal of South American Earth Sciences*, **11**(4):351-363. https://doi.org/10.1016/S0895-9811(98)00019-4

Gill R. 2009. *Igneous rocks and processes:* a practical guide. London: Wiley-Blackwell, 440 p.

Gorayeb P.S.S., Abreu F.A.M. 1989. A Faixa de Alto Grau de Cariré. *In*: Simpósio de Geologia do Nordeste, 13., Fortaleza. *Annals*... SBG-NE, p. 182-184.

Gorayeb P.S.S., Abreu, F.A.M. 1998. Granulito Macaco: nova ocorrência de rochas granulíticas na Província Borborema. *In*: SBG, Congresso Brasileiro de Geologia, Belo Horizonte. *Annals*... SBG-NE, p. 472.

Gorayeb P.S.S., Abreu F.A.M., Santos M.V., Silva Junior O.G. 2014. *Carta geológica da Folha de Sobral (SA.24-Y-D-IV), escala 1:100.000*. Brasil: Universidade Federal do Pará/CPRM – Serviço Geológico do Brasil.

Gorayeb P.S.S., Nascimento Y.E.S., Galarza M.A., Moura C.A.V. 2013. Novos dados geocronológicos do Granito do Pajé (Suíte Intrusiva Meruoca): magmatismo pós-tectônico no NW da Província Borborema. *In*: Simpósio da Província Borborema, 3., Gravatá. *Annals*... SBG-NE, p. 499.

Griffin W.L., Belousova E.A., Shee S.R., Pearson N.J., O'Reilly S.Y. 2004. Archean crustal evolution in the northern Yilgarn Craton: UePb and Hf-isotope evidence from detrital zircons. *Precambrian Research*, **131**(3-4):231-282. https://doi.org/10.1016/j.precamres.2003.12.011

Hibbard M.J. 1995. *Petrography to petrogenesis*. Englewood Cliffs: Prentice Hall, 587 p.

Jackson S.E., Pearson N.J., Griffin W.L., Belousova E.A. 2004. The application of laser ablation-inductively coupled plasma-mass spectrometry to in situ U-Pb zircon geochronology. *Chemical Geology*, **211**(1-2):47-69. https://doi.org/10.1016/j.chemgeo.2004.06.017

Kober B. 1987. Single grain evaporation combined with Pb emitter bedding $^{207}Pb/^{206}Pb$ investigations using thermal ion mass spectrometry and implications to zirconology. *Contributions to Mineralogy and Petrology*, **96**:63-71. https://doi.org/10.1007/BF00375526

Le Maitre R.W. 2002. *A classification of igneous rocks and glossary of terms*. London: Cambridge University Press, 193 p.

Ludwig K.R. 2003. *User's manual for Isoplot/Ex Version 3.2*. A geochronological toolkit for Microsoft Excel. Berkeley: Berkeley Geochronological Center Special Publication, 70 p.

Lugmair G.W., Marti K. 1978. Lunar initial 143Nd/144Nd: differential evolution of the lunar crust and mantle. *Earth and Planetary Science Letters*, **39**(3):349-357. https://doi.org/10.1016/0012-821X(78)90021-3

Martins G., Oliveira E.P., Lafon J.M. 2009. The Algodões amphibolite-tonalite gneiss sequence, Borborema Province, NE Brazil: geochemical and geocronological evidence for paleoproterozoic accretion of oceanic plateau/back-arc basalts and adakitic plutons. *Gondwana Research*, **15**(1):71-85. https://doi.org/10.1016/j.gr.2008.06.002

Mattos I.C., Nogueira Neto J.A., Artur A.C. 2017. Petrografia e química mineral do Stock Granítico Serra do Barriga (Sobral, CE, nordeste do Brasil). *Pesquisas em Geociências*, **44**(3):501-511. https://doi.org/10.22456/1807-9806.83272

Milhomem Neto J.M., Lafon J.M., Galarza M.A. 2017a. Lu-Hf em zircão por LA-MC-ICPMS no Laboratório Pará-Iso (UFPA): metodologia e primeiro exemplo de aplicação na porção sudeste do Escudo das Guianas, estado do Amapá. *In*: Contribuições à Geologia da Amazônia, 10. *Annals*... SBG-NO, p.195-208.

Milhomem Neto J.M., Lafon J.M., Galarza M.A., Moura C.A.V. 2017b. Dados Isotópicos U-Pb e Lu-Hf em zircão para o Bloco Arqueano Amapá, Sudeste do Escudo das Guianas, Norte do Brasil. *In*: Contribuições à Geologia da Amazônia, 10. *Annals*... SBG-NO, p. 333-346.

Naleto J.L.C. 2018. *Geologia e recursos minerais da Folha SA.24-Y-D-V Irauçuba*. Escala 1:100.000, Programa Geologia do Brasil. Fortaleza: CPRM, 79 p.

Neves S.P. 2012. *Granitos orogênicos:* da geração dos magmas à intrusão e deformação. Rio de Janeiro: Synergia, 148 p.

Nogueira J.F. 2004. *Estrutura, geocronologia e alojamento dos batólitos Quixadá, Quixeramobim e Senador Pompeu – Ceará Central*. PhD Thesis, Universidade Estadual de Campinas, Campinas, 123 p.

Oliveira E.C., Lafon J.M., Gioia S.M.C.L., Pimentel M.M. 2008. Datação Sm-Nd em rocha total e granada do metamorfismo granulítico da região de Tartarugal Grande, Amapá Central. *Revista Brasileira de Geociências*, **38**(1):114-127.

Patterson S.R., Vernon R.H., Tobisch O.T. 1989. A review of criteria for the identification of magmatic and tectonic foliations in granitoids. *Journal of Structural Geology*, **11**(3):349-363. https://doi.org/10.1016/0191-8141(89)90074-6

Santos T.J.S., Fetter A.H., Hackspacher P.C., Van Schmus W.R., Nogueira Neto J.A. 2008. Neoproterozoic tectonic and magmatic episodes in the NW segment of the Borborema Province, NE Brazil, during the assembly of the western Gondwana. *Journal of South American Earth Sciences*, **25**(3):271-284. https://doi.org/10.1016/j.jsames.2007.05.006

Santos T.J.S., Garcia M.G.M., Amaral W.S., Caby R., Wernick E., Arthaud M.H., Dantas E.L., Santosh M. 2009. Relics of eclogite facies assemblages in the Ceará Central Domain, NW Borborema Province, NE Brazil: implications for the assembly of West Gondwana. *Gondwana Research*, **15**(3-4):454-470. https://doi.org/10.1016/j.gr.2009.01.003

Sawyer E.W. 2008. *Atlas of migmatites*. The Canadian Mineralogist, Special Publication 9. Ottawa, Ontario, Canada: NRC Research Press. 387 p.

Spencer C.J., Kirkland C.L., Taylor R.J.M. 2016. Strategies towards statistically robust interpretations of in situ U-Pb zircon geochronology. *Geoscience Frontiers*, **7**(4):581-589. https://doi.org/10.1016/j.gsf.2015.11.006

Stacey J.S., Kramer J.D. 1975. Approximation of terrestrial lead isotope evolution by a two-stage model. *Earth Planetary Science Letters*, **26**(2):207-221. https://doi.org/10.1016/0012-821X(75)90088-6

Streckeisen A. 1976. To each plutonic rocks its proper name. *Earth Science Review*, **12**(1):1-33. https://doi.org/10.1016/0012-8252(76)90052-0

Teixeira M.F.B., Nascimento R.S., Gorayeb, P.S.S., Moura, C.A.V., Abreu F.A.M. 2010. Novos dados geocronológicos Pb-Pb em zircão do Feixe de Diques Aroeiras e sua relação com o Granito Meruoca - noroeste do Ceará. *In*: Congresso Brasileiro de Geologia, 45. *Annals*... SBG-NO, p. 1.